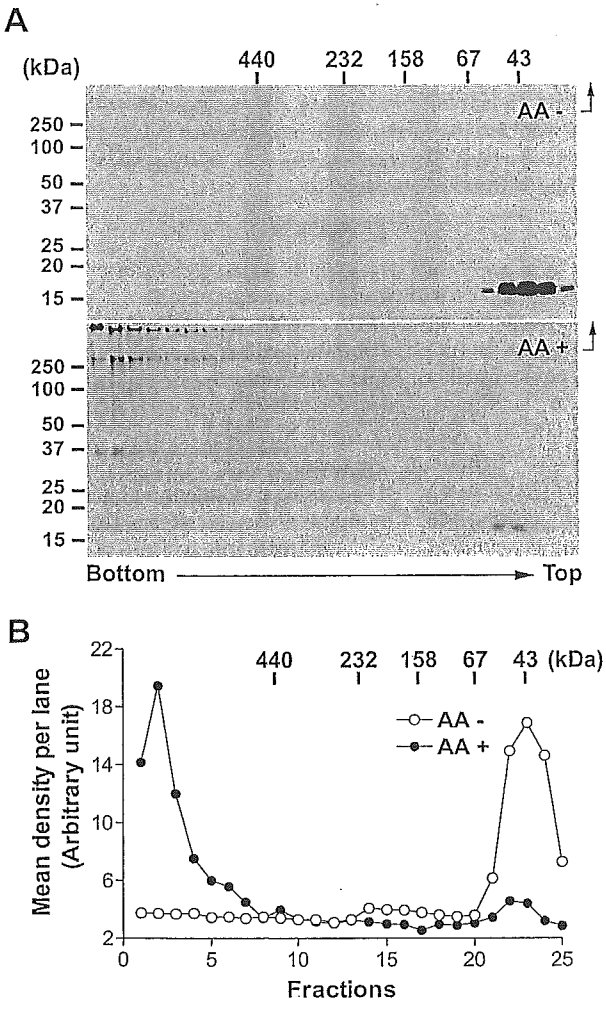

FIG. 4. **Glycerol density gradient centrifugation and densitometric analysis of SOD1 oligomers.** *A*, apo-A4V (2.5 μM) was incubated at 37 °C for 90 min in the absence or presence of 100 μM AA before loading on the glycerol cushion. After centrifugation, fractions were collected from the bottom of the tubes and then subjected to SDS-PAGE under non-reducing conditions. SOD1 proteins were detected by Western blotting. *B*, for densitometric analysis, we measured mean density per lane after background subtraction. Total mean density was similar under each condition, by calculating the mean density of visible lanes (*lanes 1–8* for oligomers and *lanes 21–25* for dimer or monomer). *Arrows* indicate the position of stacking gels.

bated in the absence of AA (Fig. 4*A*, *bottom panel*). Although oligomers of >440 kDa were fractionated by the glycerol density gradient centrifugation, these were detected as monomer, dimer, and smeared high molecular mass bands that reached stacking gels under non-reducing SDS-PAGE (Fig. 4*A*, *bottom panel*). This indicates oligomers are partly disrupted during the boiling of the SDS-PAGE loading buffer. We next performed densitometric analysis from Western blotting images to estimate the amount of oligomerized SOD1 (Fig. 4*B*). The resulting image analysis found that immunoreactivity for oligomers was ~80% of the total immunoreactivity.

Structural Instability of SOD1 Is Correlated to Oligomerization Propensity and FA Binding—We showed the FA-induced oligomerization propensity of apo-SOD1s was higher than that of holo-SOD1. This implies that protein stability might be strongly associated with FA-induced oligomerization propensity. Among the holo-enzymes, wild-type and G93A were not oligomerized under our experimental conditions (Fig. 2*B*, *top panel*). To examine the correlation between oligomerization propensity and protein stability of holo-enzymes, holo-SOD1 was heated and then oligomerized by AA. In the absence of AA,

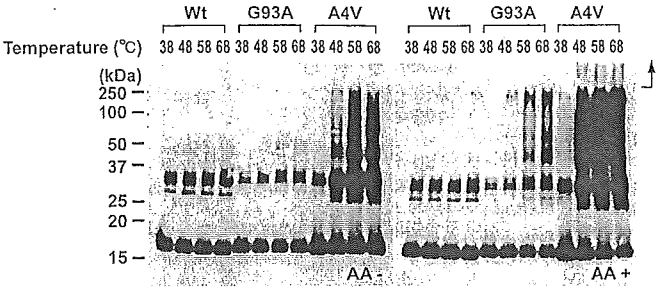

FIG. 5. **Thermally destabilized SOD1 mutants show a high oligomerization propensity.** Holo-enzymes were heat-treated at the indicated temperatures for 30 min before addition of 100 μM AA and then further incubated at 37 °C for 1 h. SDS-PAGE was performed under non-reducing conditions. Proteins were detected by Western blotting as described under "Experimental Procedures." *Arrows* indicate the position of stacking gels.

only heat-treated A4V was oligomerized (Fig. 5, *left panel*). In the presence of AA, heat-treated G93A and A4V were highly aggregated, but under the same conditions, wild-type SOD1 was not (Fig. 5, *right panel*). Oligomerization was observed above 58 °C for G93A and above 48 °C for A4V (Fig. 5, *right panel*). In the previous study, A4V was more unstable than G93A for heat treatment analyzed by differential scanning calorimetry (12). This result suggests that structural instability is strongly correlated with oligomerization propensity induced by FAs.

Although we showed that FAs promoted SOD1 oligomerization, the mechanism is not perfectly understood. Similarly, unsaturated FAs oligomerize α-synuclein and tau. In the case of α-synuclein and tau, FAs were bound to proteins, which suggested that oligomerization mechanisms underlie the FA binding characteristics of protein. To examine whether SOD1 binds to FAs, we carried out a solid-phase oleic acid binding assay. Among the holo-enzymes, very small amounts of holo-A4V were bound to the oleate-Sepharose column, whereas wild-type and G93A were not (Fig. 6*A*). All of the apo-enzymes were bound to oleate-Sepharose, regardless of their mutations (Fig. 6*A*). In contrast, bound proteins were not observed in mock-Sepharose (Fig. 6*A*). Nearly all of the input amounts of metal-deficient proteins were bound, which was estimated by 50% input. This finding suggests that metal-deficient SOD1 proteins strongly bind to FAs. We next examined whether heat-treated holo-enzymes bind to FAs. Apo-enzymes were used as control binding. Heat-treated SOD1 mutant (G93A) at 58 °C and 68 °C was bound to FAs, whereas wild-type was not (Fig. 6*B*). The results of the FA binding assay were strongly correlated with the oligomerization propensity of SOD1. These findings suggest that FA binding alters the conformation of SOD1 to form oligomers.

FA-induced SOD1 Aggregates Result in Granular Morphology and Are Cytotoxic—We analyzed the ultrastructure of SOD1 aggregates by electron microscope. SOD1 proteins (~40 μM) were incubated in the presence of 100 μM AA at 37 °C for 24 h. Holo-enzymes were heated at 50 °C for 30 min before incubation in the presence of AA. After incubation, granular aggregates were observed in all of apo-enzymes and heat-treated SOD1 mutants (Fig. 7*A*). In contrast, no visible materials were found in wild-type holo-SOD1s, even though they were heat-treated (Fig. 7*A*). The morphology of the aggregates was round or amorphous large granules composed of clustered small granules (Fig. 7*A*). We could not observe any visible protein aggregates in the samples incubated without AA, except in apo-A4V, which revealed a fibril structure (data not shown).

We next examined the effect of FA-induced aggregates on cell

viability of differentiated neuro2a cells. Aggregates of SOD1s were formed using the same methods as described for observation under an electron microscope. Aliquots incubated in the presence or absence of AA were diluted in the culture medium, which was directly added to differentiated neuro2a cells. After incubation for 18 h, toxicity was assessed with MTS reduction (Fig. 7*B*) and trypan blue staining (Fig. 7*C*). The presence of the granular aggregates formed by AA from Apo-SOD1s and heat-treated SOD1 mutants significantly reduced cell viability (Fig. 7, *B* and *C*). In contrast, no significant decrease of viability was detected when the cells were exposed either to incubated proteins in the absence of AA or to the buffer solutions used to form the aggregates in the absence of added protein (Fig. 7, *B* and *C*). These findings suggest that FA-induced SOD1 aggregates were highly toxic to the cells.

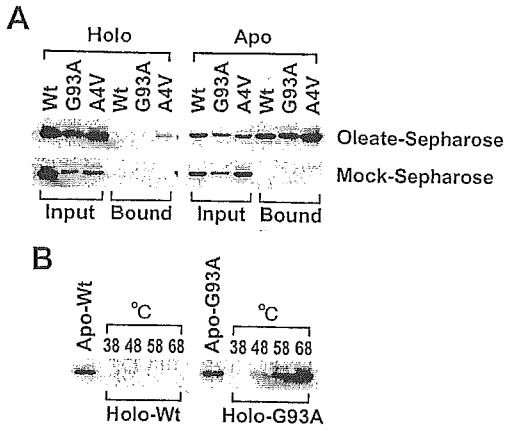

FIG. 6. **Solid-phase oleic acid binding assay shows apo-SOD1 or thermally destabilized SOD1 bound to oleate-Sepharose.** *A*, solid-phase binding assay was performed as described under "Experimental Procedures." Approximately 50% input (100 ng of proteins) was electrophoresed to estimate the quantity of FA binding SOD1. *B*, holo-SOD1s (wild-type and G93A) were thermally destabilized at the indicated temperatures for 30 min and then directly loaded on oleate-Sepharose. Apo-enzymes were used as positive controls for oleic acid binding.

DISCUSSION

Numerous neurodegenerative diseases are accompanied by highly insoluble inclusions of protein aggregates within characteristic neuronal populations. In the case of FALS, the protypical Lewy body-like hyaline inclusions, composed largely of granule-coated fibrils of SOD1-insoluble filaments, have been detected in the spinal cord of FALS patients with SOD1 gene mutations (5, 28). Although there has been controversy about whether such inclusions are a cause or a consequence of the neuronal degeneration, accumulating evidence suggests that aggregates formed via misfolded proteins, especially soluble oligomeric assemblies, may cause cell injury (29–31). Moreover, cytotoxicity of protein aggregates may have common features because granular aggregates form non-pathological proteins that can also be toxic (26). These findings suggest the avoidance of protein aggregation may be crucial for therapy of

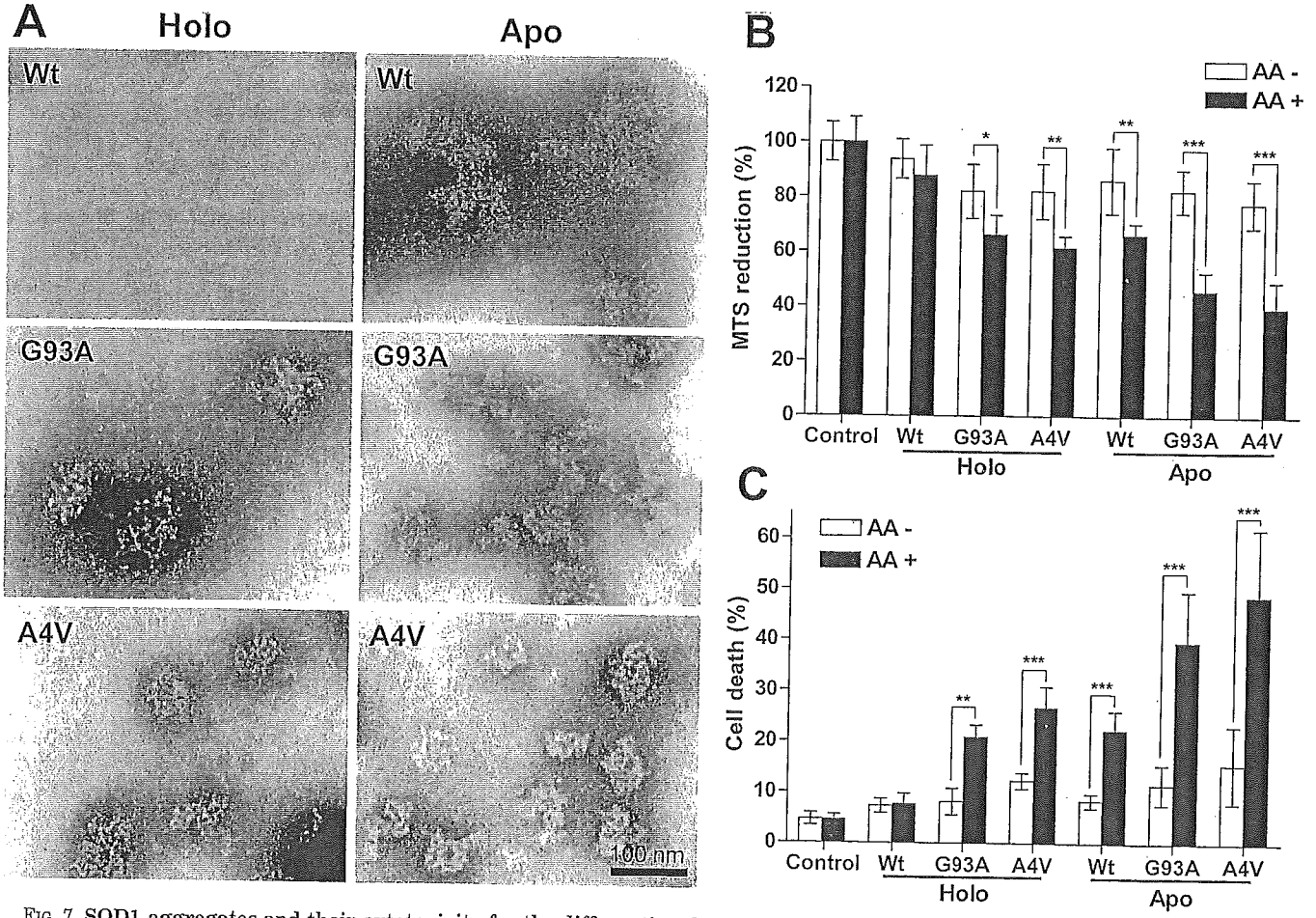

FIG. 7. **SOD1 aggregates and their cytotoxicity for the differentiated neuro2a cells.** Holo-SOD1s were pre-heated at 50 °C for 30 min before incubation with AA. SOD1 proteins (40 μM) were incubated in the presence of 100 μM AA at 37 °C for 24 h before observation under an electron microscope (*A*). Differentiated neuro2a cells were directly exposed for 18 h in medium containing incubated aliquots of SOD1s with or without arachidonic acid. The concentration of SOD1 in the culture medium was 4 μM. Buffer and AA carryover in the culture medium was controlled. Cytotoxicity was assessed using an MTS reduction assay (*B*) and trypan blue exclusion staining (*C*). The results were analyzed by two-way analysis of variance. The values are the means ± S.D. ($n = 6$). *, $p < 0.05$; **, $p < 0.01$; ***, $p < 0.001$.

conformational diseases including FALS.

In the present study, we demonstrated that unsaturated FAs promoted SOD1 oligomerization at physiological pH. SOD1 oligomers were detected by SDS-PAGE under non-reducing conditions. Although immunoreactivity for SOD1 oligomers was decreased in SDS-PAGE under reducing conditions, SOD1 oligomers were considerably SDS-resistant under non-reducing conditions. Based on this method, we found that apo-SOD1 proteins were highly oligomerized by AA compared with holo-SOD1 proteins in time-dependent and FA concentration-dependent manners (Fig. 2, *B* and *C*). Metal-deficient SOD1s may be representative of misfolding intermediates for their oligomeric assemblies because they are oligomerized independent of their mutations. These findings suggest that metal-deficient SOD1 proteins have a high oligomerization propensity, which is consistent with previous studies (9, 10, 13, 32). Moreover, heating of holo-SOD1 mutants increased the tendency to form oligomer complexes, especially in the presence of AA; however, the wild-type holo-SOD1 did not form oligomers, even after heating to 68 °C and exposure to AA (Fig. 5). This finding suggests that mutations of SOD1 primarily affect their conformation. Our time-course analysis of oligomerization demonstrates that FAs induced the oligomerization process fairly rapidly. We could detect oligomers within 1 h of incubation in the presence of AA (Fig. 1*C*). Glycerol density gradient centrifugation analysis showed that oligomer species were roughly estimated to be >80% of the total SOD1 after a 90-min incubation in the presence of AA (Fig. 4). The conversion efficiency and the speed of oligomer formation may be considered as supportive evidence that these reactions occur *in vivo*.

Aggregations of misfolded proteins are primarily affected by their mutations, especially in inherited conformational diseases. Mutant proteins in conformational diseases have a common characteristic of easily unfolding in a physiological condition and favoring aggregate formation. Protein aggregation has also been shown to be modulated by several factors, including protein concentration, pH, and interactions with other elements such as lipid molecules. It has been reported that FAs stimulated the polymerization of amyloid β-peptides, tau (17, 33), and α-synuclein (18, 19) *in vitro*. These studies suggest that FAs play a pivotal role as nucleates in the self-assembly of misfolded proteins. Although the precise mechanism of how lipid molecules accelerate protein aggregation has not been elucidated, it has been proposed that lipid-bound proteins change their conformation or anionic surfaces, presenting as micelles or vesicles, which can serve to nucleate aggregate formation (18, 34, 35). We confirmed that apo-SOD1s or heat-treated holo-SOD1 mutants were bound to oleic acid (Fig. 6). The FA binding properties of SOD1s were strongly correlated to their conformational instability. These results are consistent with the notion that misfolding intermediates of SOD1 caused by mutations or metal loss may be facilitated by FAs to form oligomeric structures. Another possible mechanism is protein oxidation by FAs. Oxidation also enhances misfolding and aggregation of SOD1 (32). In particular, FAs can lead to the production of radicals because they are easily peroxidized by auto-oxidation to generate peroxyl radicals. However, we could not inhibit SOD1 oligomerization using even a considerable amount of radical scavenger (data not shown). Moreover, oxidized derivatives of FAs also induced SOD1 oligomerization to a similar extent with fresh FAs (data not shown). This finding suggests that oxidation or oxidative damage of SOD1 does not directly drive SOD1 oligomerization. Rather, it is most likely to be associated with a SOD1-destabilizing event.

Recently, several studies for *in vitro* aggregation of SOD1 have been published. Aggregation of SOD1 can be induced by metal-catalyzed oxidation (32), trifluoroethanol, or heat treatment (10), which induces oxidative modification or protein destabilization. This indicates that structurally unstable SOD1 has an influence on its aggregate formation *in vitro*. Crystallographic studies suggest that metal-deficient SOD1 forms an amyloid-like assembly caused by non-native conformational changes and permits dimer interaction (36, 37). This amyloid-like structure was represented by prolonged incubation of SOD1 at acidic pH (9). In the present study, ultrastructural analysis showed that the FA-inducing aggregates had round or amorphous morphology with clustered tiny spherical aggregates (Fig. 7*A*). They resemble pre-fibrillar aggregates of the N-terminal domain of *Escherichia coli* HypF protein or aggregates of the Src homology 3 domain of cytosolic phosphatidylinositol 3-kinase as reported by Stefani and co-workers (26). They demonstrated that granular aggregates of proteins, even non-pathological proteins, are cytotoxic when applied externally (26). Our data also demonstrate that granular aggregates of SOD1s reveal significant cytotoxicity (Fig. 7, *B* and *C*). Although the cytotoxic mechanism of the aggregates is not completely understood, it has been proposed that such pre-fibrillar intermediates may lead to cytotoxicity by permeabilization of the membrane bilayer (38, 39).

The present findings may provide considerable pathological implication for FALS. Lipid molecules such as FAs may be positive modulators for misfolded protein aggregations. Most misfolded proteins including SOD1 mutants are rapidly degraded by the ubiquitin-proteasome system. Unsaturated FAs may promote misfolded protein aggregations before they are degraded. In addition, cytotoxic aggregate formation of SOD1 may require FAs because granular aggregates structures were markedly observed in SOD1s incubated with AA. Although it is not clear whether the cytotoxic aggregates of SOD1s are generated intracellularly, we have provided a protein aggregation model system to help understand the pathological significance of FAs as a positive modulator for the aggregate formation in FALS. We believe that our system will contribute to efficient drug screening for inhibitors of SOD1 aggregation.

Acknowledgment—We thank Dr. Toshihide Kobayashi for critical advice and helpful discussions.

REFERENCES

1. Deng, H. X., Hentati, A., Tainer, J. A., Iqbal, Z., Cayabyab, A., Hung, W. Y., Getzoff, E. D., Hu, P., Herzfeldt, B., Roos, R. P., Warner, C., Deng, G., Soriano, E., Smyth, C., Parge, H. E., Ahmed, A., Roses, A. D., Hallewell, R., Pericak-Vance, M. A., and Siddique, T. (1993) *Science* **261**, 1047–1051
2. Rosen, D. R., Siddique, T., Patterson, D., Figlewicz, D. A., Sapp, P., Hentati, A., Donaldson, D., Goto, J., O'Regan, J. P., Deng, H. X., Rahmani, Z., Krizus, A., McKenna-Yasek, D., Cayabyab, A., Gaston, S., Tanzi, R., Halperin, J. J., Herzfeldt, B., Van den Berg, R., Hung, W., Bird, T., Deng, G., Mulder, D. W., Smith, C., Laing, N. G., Soriano, E., Pericak-Vance, M. A., Haines, J., Rouleau, G. A., Gusella, J., Horvitz, H. R., and Brown, R. H., Jr. (1993) *Nature* **362**, 59–62
3. Shibata, N., Asayama, K., Hirano, A., and Kobayashi, M. (1996) *Dev. Neurosci.* **18**, 492–498
4. Bruijn, L. I., Becher, M. W., Lee, M. K., Anderson, K. L., Jenkins, N. A., Copeland, N. G., Sisodia, S. S., Rothstein, J. D., Borchelt, D. R., Price, D. L., and Cleveland, D. W. (1997) *Neuron* **18**, 327–338
5. Kato, S., Hayashi, H., Nakashima, K., Nanba, E., Kato, M., Hirano, A., Nakano, I., Asayama, K., and Ohama, E. (1997) *Am. J. Pathol.* **151**, 611–620
6. Shibata, N., Hirano, A., Kobayashi, M., Dal Canto, M. C., Gurney, M. E., Komori, T., Umahara, T., and Asayama, K. (1998) *Acta Neuropathol.* **95**, 136–142
7. Watanabe, M., Dykes-Hoberg, M., Culotta, V. C., Price, D. L., Wong, P. C., and Rothstein, J. D. (2001) *Neurobiol. Dis.* **8**, 933–941
8. Wang, J., Xu, G., Gonzales, V., Coonfield, M., Fromholt, D., Copeland, N. G., Jenkins, N. A., and Borchelt, D. R. (2002) *Neurobiol. Dis.* **10**, 128–138
9. DiDonato, M., Craig, L., Huff, M. E., Thayer, M. M., Cardoso, R. M., Kassmann, C. J., Lo, T. P., Bruns, C. K., Powers, E. T., Kelly, J. W., Getzoff, E. D., and Tainer, J. A. (2003) *J. Mol. Biol.* **332**, 601–615
10. Stathopulos, P. B., Rumfeldt, J. A., Scholz, G. A., Irani, R. A., Frey, H. E., Hallewell, R. A., Lepock, J. R., and Meiering, E. M. (2003) *Proc. Natl. Acad. Sci. U. S. A.* **100**, 7021–7026
11. Hayward, L. J., Rodriguez, J. A., Kim, J. W., Tiwari, A., Goto, J. J., Cabelli, D. E., Valentine, J. S., and Brown, R. H., Jr. (2002) *J. Biol. Chem.* **277**, 15923–15931

12. Rodriguez, J. A., Valentine, J. S., Eggers, D. K., Roe, J. A., Tiwari, A., Brown, R. H., Jr., and Hayward, L. J. (2002) *J. Biol. Chem.* **277,** 15932–15937
13. Lindberg, M. J., Tibell, L., and Oliveberg, M. (2002) *Proc. Natl. Acad. Sci. U. S. A.* **99,** 16607–16612
14. Johnston, J. A., Dalton, M. J., Gurney, M. E., and Kopito, R. R. (2000) *Proc. Natl. Acad. Sci. U. S. A.* **97,** 12571–12576
15. Urushitani, M., Kurisu, J., Tateno, M., Hatakeyama, S., Nakayama, K., Kato, S., and Takahashi, R. (2004) *J. Neurochem.* **90,** 231–244
16. Shinder, G. A., Lacourse, M. C., Minotti, S., and Durham, H. D. (2001) *J. Biol. Chem.* **276,** 12791–12796
17. Wilson, D. M., and Binder, L. I. (1997) *Am. J. Pathol.* **150,** 2181–2195
18. Sharon, R., Goldberg, M. S., Bar-Josef, I., Betensky, R. A., Shen, J., and Selkoe, D. J. (2001) *Proc. Natl. Acad. Sci. U. S. A.* **98,** 9110–9115
19. Sharon, R., Bar-Joseph, I., Frosch, M. P., Walsh, D. M., Hamilton, J. A., and Selkoe, D. J. (2003) *Neuron* **37,** 583–595
20. Urushitani, M., Kurisu, J., Tsukita, K., and Takahashi, R. (2002) *J. Neurochem.* **83,** 1030–1042
21. Fried, R. (1975) *Biochimie (Paris)* **57,** 657–660
22. Crow, J. P., Sampson, J. B., Zhuang, Y., Thompson, J. A., and Beckman, J. S. (1997) *J. Neurochem.* **69,** 1936–1944
23. Boissinot, M., Karnas, S., Lepock, J. R., Cabelli, D. E., Tainer, J. A., Getzoff, E. D., and Hallewell, R. A. (1997) *EMBO J.* **16,** 2171–2178
24. Bartnikas, T. B., and Gitlin, J. D. (2003) *J. Biol. Chem.* **278,** 33602–33608
25. Peters, T., Jr., Taniuchi, H., and Anfinsen, C. B., Jr. (1973) *J. Biol. Chem.* **248,** 2447–2451
26. Bucciantini, M., Giannoni, E., Chiti, F., Baroni, F., Formigli, L., Zurdo, J., Taddei, N., Ramponi, G., Dobson, C. M., and Stefani, M. (2002) *Nature* **416,** 507–511
27. Kayed, R., Head, E., Thompson, J. L., McIntire, T. M., Milton, S. C., Cotman, C. W., and Glabe, C. G. (2003) *Science* **300,** 486–489
28. Kato, S., Saito, M., Hirano, A., and Ohama, E. (1999) *Histol. Histopathol.* **14,** 973–989
29. Walsh, D. M., Hartley, D. M., Kusumoto, Y., Fezoui, Y., Condron, M. M., Lomakin, A., Benedek, G. B., Selkoe, D. J., and Teplow, D. B. (1999) *J. Biol. Chem.* **274,** 25945–25952
30. Hartley, D. M., Walsh, D. M., Ye, C. P., Diehl, T., Vasquez, S., Vassilev, P. M., Teplow, D. B., and Selkoe, D. J. (1999) *J. Neurosci.* **19,** 8876–8884
31. Tateno, M., Sadakata, H., Tanaka, M., Itohara, S., Shin, R. M., Miura, M., Masuda, M., Aosaki, T., Urushitani, M., Misawa, H., and Takahashi, R. (2004) *Hum. Mol. Genet.* **13,** 2183–2196
32. Rakhit, R., Cunningham, P., Furtos-Matei, A., Dahan, S., Qi, X. F., Crow, J. P., Cashman, N. R., Kondejewski, L. H., and Chakrabartty, A. (2002) *J. Biol. Chem.* **277,** 47551–47556
33. Gamblin, T. C., King, M. E., Kuret, J., Berry, R. W., and Binder, L. I. (2000) *Biochemistry* **39,** 14203–14210
34. Necula, M., Chirita, C. N., and Kuret, J. (2003) *J. Biol. Chem.* **278,** 46674–46680
35. Chirita, C. N., Necula, M., and Kuret, J. (2003) *J. Biol. Chem.* **278,** 25644–25650
36. Elam, J. S., Taylor, A. B., Strange, R., Antonyuk, S., Doucette, P. A., Rodriguez, J. A., Hasnain, S. S., Hayward, L. J., Valentine, J. S., Yeates, T. O., and Hart, P. J. (2003) *Nat. Struct. Biol.* **10,** 461–467
37. Strange, R. W., Antonyuk, S., Hough, M. A., Doucette, P. A., Rodriguez, J. A., Hart, P. J., Hayward, L. J., Valentine, J. S., and Hasnain, S. S. (2003) *J. Mol. Biol.* **328,** 877–891
38. Caughey, B., and Lansbury, P. T. (2003) *Annu. Rev. Neurosci.* **26,** 267–298
39. Kayed, R., Sokolov, Y., Edmonds, B., McIntire, T. M., Milton, S. C., Hall, J. E., and Glabe, C. G. (2004) *J. Biol. Chem.* **279,** 46363–46366

Inactivation of *Drosophila* DJ-1 leads to impairments of oxidative stress response and phosphatidylinositol 3-kinase Akt signaling

Yufeng Yang*†, Stephan Gehrke*†, Md. Emdadul Haque*, Yuzuru Imai*, Jon Kosek*, Lichuan Yang‡, M. Flint Beal‡, Isao Nishimura§, Kazumasa Wakamatsu¶, Shosuke Ito¶, Ryosuke Takahashi, and Bingwei Lu*,**

*Department of Pathology, Stanford University School of Medicine, and Geriatric Research, Education and Clinical Center Veterans Affairs Palo Alto Health Care System, Palo Alto, CA 94304; ‡Department of Neurology, Cornell University Medical College, 525 East 68th Street, New York, NY 10021; §Division of Regulation of Macromolecular Functions, Institute for Protein Research, Osaka University, 3-2 Yamadaoka, Suita, Osaka 565-0871, Japan; ¶Department of Chemistry, Fujita Health University School of Health Sciences, Toyoake, Aichi 470-1192, Japan; and Laboratory for Motor System Neurodegeneration, RIKEN Brain Science Institute, 2-1 Hirosawa, Wako-shi, Saitama 351-0198, Japan

Edited by Tak Wah Mak, University of Toronto, Toronto, Canada, and approved July 29, 2005 (received for review June 3, 2005)

Parkinson's disease (PD) is the most common movement disorder characterized by dopaminergic dysfunction and degeneration. The cause of most PD cases is unknown, although postmortem studies have implicated the involvement of oxidative stress. The identification of familial PD-associated genes offers the opportunity to study mechanisms of PD pathogenesis in model organisms. Here, we show that DJ-1A, a *Drosophila* homologue of the familial PD-associated gene DJ-1, plays an essential role in oxidative stress response and neuronal maintenance. Inhibition of DJ-1A function through RNA interference (RNAi) results in cellular accumulation of reactive oxygen species, organismal hypersensitivity to oxidative stress, and dysfunction and degeneration of dopaminergic and photoreceptor neurons. To identify other genes that may interact with DJ-1A in regulating cell survival, we performed genetic interaction studies and identified components of the phosphatidylinositol 3-kinase (PI3K) Akt-signaling pathway as specific modulators of DJ-1A RNAi-induced neurodegeneration. PI3K signaling suppresses DJ-1A RNAi phenotypes at least in part by reducing cellular reactive oxygen species levels. Consistent with the genetic interaction results, we also found reduced phosphorylation of Akt in DJ-1A RNAi animals, indicating an impairment of PI3K Akt signaling by DJ-1A down-regulation. Together with recent findings in mammalian systems, these results implicate impairments of PI3K Akt signaling and oxidative stress response in DJ-1-associated disease pathogenesis. We also observed impairment of PI3K Akt signaling in the fly *parkin* model of PD, hinting at a common molecular event in the pathogenesis of PD. Manipulation of PI3K Akt signaling may therefore offer therapeutic benefits for the treatment of PD.

Parkinson's disease PI3K PTEN Akt signaling reactive oxygen species.

Parkinson's disease (PD) is the most common movement disorder and the second most common neurodegenerative disease. The movement abnormality in PD arises from deficiency of brain dopamine (DA) contents and the degeneration of dopaminergic neurons in the substantia nigra. The most common forms of PD are sporadic with no known cause. Nevertheless, postmortem studies have identified common features associated with sporadic PD, including defects in mitochondrial complex I function, oxidative damage, and abnormal protein aggregation (1).

The contribution of genetic factors in the pathogenesis of PD, although initially controversial, has been firmly established by recent human genetic studies. At least 10 distinct loci (PARK1 to -11) have been linked to rare familial forms of PD (2). It is anticipated that understanding the molecular lesions associated with these familial PD (FPD) genes will shed light on the pathogenesis of the sporadic forms of the disease. To date, five unequivocal FPD genes have been molecularly cloned. These include -*Synuclein* (-Syn), Parkin, DJ-1, PINK-1, and dardarin. Biochemical and biophysical studies of -Syn and Parkin have primarily linked dysfunction of these genes to aberrant protein folding and ubiquitin-proteasome dysfunction. Intriguingly, *in vivo* genetic and *in vitro* cell culture studies have revealed their connection to mitochondrial dysfunction and oxidative stress, reinforcing the involvement of these processes in PD pathogenesis in general (3).

DJ-1 encodes a conserved protein belonging to the ThiJ PfpI DJ-1 superfamily. The exact molecular function of DJ-1 is still unclear. Human DJ-1 was initially discovered as a candidate oncoprotein that could transform cells in cooperation with activated *ras* (4), and it was later found as a component of an RNA-binding protein complex and was associated with male infertility (4–6). Under oxidative stress conditions, DJ-1 was modified by oxidation, and the modified form associated with mitochondria in cultured cells (7–10). Knocking down DJ-1 expression with small interfering RNA (siRNA) resulted in susceptibility to oxidative stress, endoplasmic reticulum stress, and proteasome inhibition (11). Recent analyses of DJ-1 knockout mice have shed light on the physiological function of DJ-1 in mammals. DJ-1-deficient mice were found to have nigrostriatal dopaminergic dysfunction, motor deficits, and hypersensitivity to the neurotoxin 1-methyl-4-phenyl-1,2,3,6-tetrahydropyrindine (MPTP) and oxidative stress stimuli (12–14). In mammalian cells, DJ-1 was found to regulate the phosphorylation status of protein kinase B (PKB) Akt through the tumor suppressor PTEN (15). The relevance of this novel finding of DJ-1 function to PD pathogenesis remains to be explored.

As an alternative approach to understanding the role of DJ-1 dysfunction in PD pathogenesis, we have used *Drosophila* as a model system. We inhibited the function of a *Drosophila* DJ-1 homologue (DJ-1A) by transgenic RNA interference (RNAi). DJ-1A RNAi flies show cellular accumulation of reactive oxygen species (ROS), hypersensitivity to oxidative stress, and degeneration of dopaminergic and photoreceptor neurons. Genetic interaction studies with candidate genes and pathways previously implicated in survival signaling led to the identification of genes in the PI3K Akt-signaling pathway as specific modifiers of DJ-1A-associated cell death phenotype. Consistent with the genetic interaction results, PI3K signaling was found to regulate cellular ROS levels, and we found that DJ-1A down-regulation leads to impairment of PI3K Akt signaling. Significantly, we found that dysfunction of *parkin*, another PD-associated gene, also led to impaired

This paper was submitted directly (Track II) to the PNAS office.

Abbreviations: DA, dopamine; DMC, dorsomedial cluster; PD, Parkinson's disease; RNAi, RNA interference; ROS, reactive oxygen species; TH, tyrosine hydroxylase; PKB, protein kinase B; PI3K, phosphatidylinositol 3-kinase; *Da*, *daughterless*; 3-AT, 3-amino-triazole; DCFH-DA, 2,7-dichlorofluorescein diacetate; DN, dominant-negative.

†Y.Y. and S.G. contributed equally to this work.

**To whom correspondence should be addressed. E-mail: bingwei@stanford.edu.

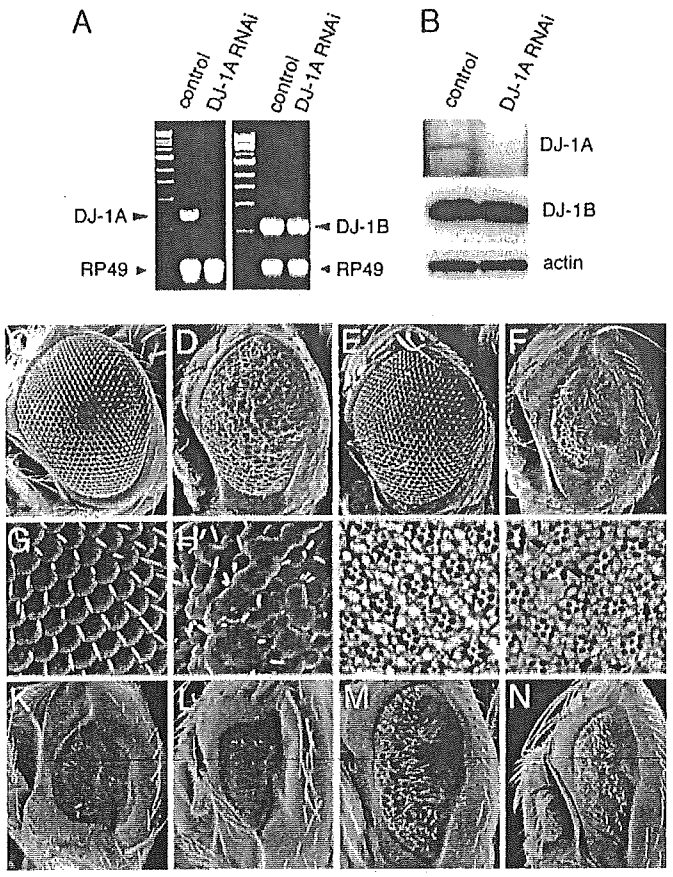

Fig. 1. Inhibition of *DJ-1A* expression by RNAi leads to photoreceptor neuron loss and eye degeneration. (*A*) Quantitative RT PCR analysis of *DJ-1A* mRNA level after RNAi. *DJ-1B* and *RP49* serve as controls. (*B*) Western blot analysis of DJ-1A protein level after RNAi. DJ-1B and actin serve as controls. (*C–H*) SEM images of *GMR-GAL4* (*C*), *GMR-GAL4 UAS-DJ-1A-RNAi* (*D*), *GMR-GAL4 Df(2R)CX1* (*E*), and *GMR-GAL4 UAS-DJ-1A-RNAi Df(2R)CX1* (*F*) eyes. *Df(2R)CX1* is a chromosomal deficiency that deletes *DJ-1A*. *G* and *H* are magnified views of *C* and *D*, respectively. (*I* and *J*) Staining of photoreceptor neurons in *GMR-GAL4* (*I*), and *GMR-GAL4 UAS-DJ-1A-RNAi* (*J*) eyes. Arrows in *J* mark ommatidia with photoreceptor loss. (*K–N*) Rescue of DJ-1A RNAi phenotypes by overexpressing *DJ-1A* or human *DJ-1*. All flies are homozygous for a recombinant *GMR-GAL4;UAS-DJ-1A-RNAi* chromosome and thus have a stronger phenotype than the one shown in *B*. In addition, the flies coexpress *UAS-GFP* (*L*), *UAS-DJ-1A* (*M*), *UAS-hDJ-1* (*N*), or no other transgene (*K*).

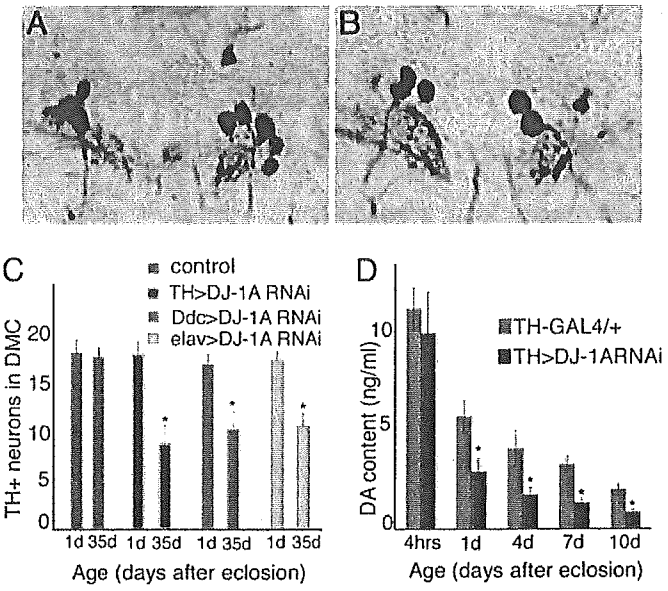

Fig. 2. Dopaminergic defects in *DJ-1A RNAi* flies. (*A* and *B*) TH immunostaining of DMC dopaminergic neurons in 35-day-old control *Ddc-GAL4* (*A*) and *Ddc-GAL4 DJ-1A RNAi* (*B*) male flies. Sections containing most of the DMC dopaminergic neurons are shown. (*C*) Quantification of TH neurons in the DMC of control flies and *DJ-1A RNAi* flies directed with *TH-GAL4*, *Ddc-GAL4*, or *elav-GAL4* drivers. The difference in cell count between 1-day-old and 35-day-old *DJ-1A RNAi* flies is significant. *, P 0.01 in Student's t test. (*D*) Quantification of head DA levels in *TH-GAL4* and *TH-GAL4 DJ-1A RNAi* flies. *, P 0.01 in Student's t test.

inducing RNAi with the *Ddc-GAL4* driver. We focused on the dopaminergic neurons in the dorsomedial clusters (DMC), which are known to be susceptible under disease conditions (26). Immunostaining of paraffin brain sections of *Ddc-GAL4 DJ-1A RNAi* flies revealed an age-dependent reduction in the number of TH neurons in the DMC. In 1-day-old flies, a normal complement of TH neurons (18) was present (Fig. 2*C*), but, in 35-day and older flies, only 10–12 of these neurons could be detected immunochemically (Fig. 2 *B* and *C*). Control flies showed no significant change in the number of these neurons during aging (Fig. 2 *A* and *C*). Induction of DJ-1A RNAi with another dopaminergic GAL4 driver, *TH-GAL4*, or the pan-neuronal *elav-GAL4* driver also resulted in reduction of TH neurons in the DM clusters (Fig. 2*C*).

To further confirm that loss of DJ-1A leads to dopaminergic dysfunction, we measured brain DA levels using head extracts prepared from control and *DJ-1A RNAi* flies. In newly eclosed flies, DA content was comparable between control and *RNAi* flies (Fig. 2*D*). However, 1 day after eclosion, *DJ-1A RNAi* flies showed significantly reduced DA level than control flies. At 4, 7, and 10 days of age, control and *DJ-1A RNAi* flies both showed age-dependent decline of DA, but *DJ-1A RNAi* flies consistently exhibited more reduction than the controls (Fig. 2*D*). Because a normal complement of TH dopaminergic neurons was present in 1-day old flies, the reduction of brain DA content at this early stage could not be attributed to neuronal loss. This result suggests that, in addition to promoting dopaminergic neuron survival, *Drosophila* DJ-1A may play an early role in regulating brain DA levels.

***DJ-1A RNAi* Flies Show Elevated ROS Accumulation and Hypersensitivity to Oxidative Stress.** We further characterized the *DJ-1A RNAi* animals to learn DJ-1A function *in vivo*. Human DJ-1 was previously found to respond to oxidative stress (8). This finding prompted us to analyze the response of *DJ-1A RNAi* flies under oxidative conditions. We used the *elav*-GAL4 driver to systematically induce DJ-1A RNAi in postmitotic neurons of transgenic flies and examined the response of these flies to treatment with exogenous H_2O_2. When treated with 1% H_2O_2, the time to reach 50% mortality was shortened by 27% in *DJ-1A RNAi* flies than control flies (Fig. 3*A*). This finding suggests that neuronal DJ-1A is important in fending off H_2O_2-induced lethality. To further confirm the sensitivity of *DJ-1A RNAi* flies to intracellular H_2O_2 levels, we treated DJ-1A RNAi flies with 3-AT, a known inhibitor of catalase, which converts H_2O_2 to H_2O. DJ-1A RNAi flies were found to be more sensitive to 3-AT treatment than the control flies (Fig. 3*B*). To test whether DJ-1A may be actively involved in ROS scavenging, we also overexpressed DJ-1A ubiquitously with the Da-GAL4 driver and observed that DJ-1A overexpression was sufficient to confer resistance against 3-AT treatment (Fig. 6, which is published as supporting information on the PNAS web site).

If DJ-1A normally plays a critical role in sensing cellular ROS levels and eliciting protective responses to remove these toxic agents, one would predict that inhibiting DJ-1A function would lead to elevated levels of endogenous ROS. We tested this possibility by staining cultured neurons with DCFH-DA, which is an indicator of hydroxyl free radicals. Compared with control neuronal culture,

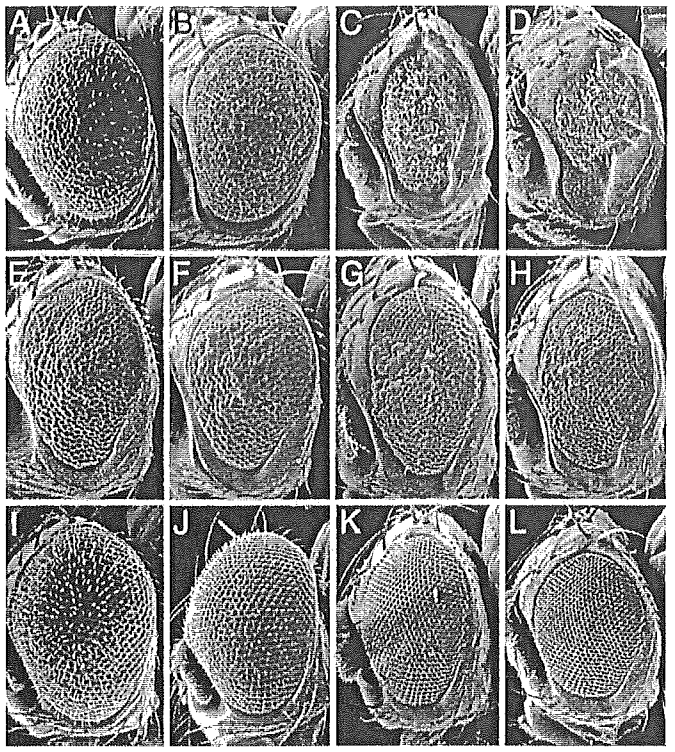

Fig. 4. Modification of DJ-1A RNAi phenotypes by altered expression of genes in the PI3K Akt pathway. (*A–D*) SEM eye images of DJ-1A RNAi flies coexpressing *UAS-Akt* (*A*), *UAS-PI3K Dp110* (*B*), *UAS-PI3K Dp110DN* (*C*), or *UAS-PTEN* (*D*). (*E–H*) SEM eye images of human tauV337M transgenic flies coexpressing *UAS-GFP* (*E*), *UAS-PI3K Dp110* (*F*), *UAS-PI3K Dp110DN* (*G*), or *UAS-PTEN* (*H*). (*I–L*) SEM eye images of flies expressing *UAS-Akt* (*I*), *UAS-PI3K Dp110* (*J*), *UAS-PI3K Dp110DN* (*K*), or *UAS-PTEN* (*L*) transgenes alone. *GMR-GAL4* was used to direct *UAS* transgene expression in all panels.

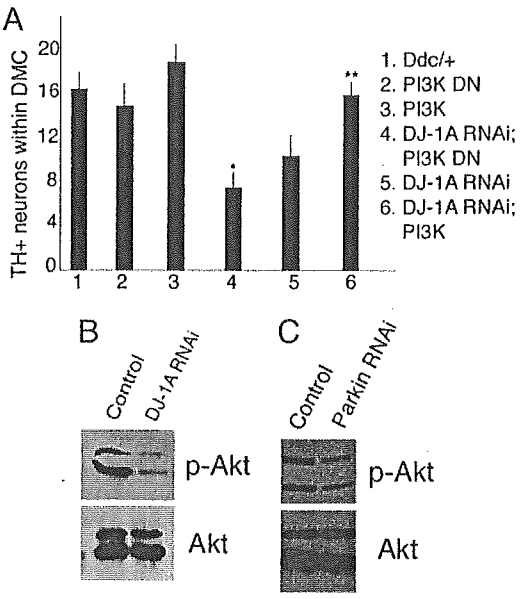

Fig. 5. Modification of DJ-1A RNAi-induced dopaminergic phenotype by altered expression of *PI3K Akt* pathway genes and Western blot analysis showing reduced Akt phosphorylation after DJ-1A or Parkin down-regulation. (*A*) Quantification of TH DA neurons in the DMC of *Ddc-GAL4* control flies, *DJ-1A RNAi* flies, *PI3K* or *PI3K DN* single overexpression flies, and *DJ-1A RNAi* flies coexpressing *PI3K* or *PI3K DN* transgenes. *, P 0.01 in Student's t test. *Ddc-GAL4* was used to direct transgene expression. (*B* and *C*) Western blot analysis of fly head extracts prepared from *Da-GAL4* and *Da-GAL4 DJ-1A RNAi* (*B*) or *Da-GAL4* and *Da-GAL4 dParkin RNAi* (*C*) genotyped flies. Blots were probed with anti-phospho-Akt and anti-Akt antibodies, respectively.

situation, coexpression of wild-type *PI3K*, *PI3K DN*, or *PTEN* showed little effect on human tau-induced toxicity in the eye (Fig. 4, compare *F*, *G*, and *H*, respectively, with *E*). The genetic interaction between DJ-1A and PI3K pathway genes in the eye thus seems to be rather specific.

We next tested the effects of modulating PI3K signaling on the dopaminergic degeneration phenotype induced by DJ-1A RNAi. Coexpression of PI3K completely suppressed the reduction of TH DA neuron phenotype induced by DJ-1A RNAi. The number of DA neurons in the DMCs was maintained at the wild-type level in all of the transgenic flies and at all ages examined (Fig. 5*A*), indicating that coexpression of PI3K blocked DJ-1A RNAi-induced age-dependent dopaminergic degeneration. Conversely, coexpression of PI3K DN showed a statistically significant enhancement of DJ-1A RNAi toxicity in dopaminergic neurons (Fig. 5*A*).

We next examined the effect of PI3K signaling on DJ-1A RNAi-induced ROS accumulation. We found that, in adult fly brain, induction of DJ-1A RNAi within dopaminergic neurons led to an elevation of ROS levels, consistent with neuronal culture studies described earlier (Fig. 7*A*, which is published as supporting information on the PNAS web site). Inhibition of PI3K signaling in these neurons by means of overexpression of PI3K DN also led to elevation of ROS levels (Fig. 7*B*), whereas flies overexpressing wild-type PI3K showed basal ROS levels (Fig. 7*C*). Strikingly, in DJ-1A RNAi flies coexpressing PI3K, cellular ROS levels are reduced to baseline levels as in wild-type controls (Fig. 7*G*). Together, these results indicate that PI3K signaling specifically suppresses DJ-1A RNAi-induced neurotoxicity and that this suppression is correlated with a reduction of cellular ROS levels.

DJ-1A RNAi Flies and Parkin Mutant Flies Exhibit Impaired PI3K Akt Signaling. The fact that increased PI3K Akt signaling specifically suppressed DJ-1A RNAi-induced cell death suggests that the cell death in DJ-1A RNAi animals may be caused by a reduction of PI3K Akt signaling. To test this possibility, we examined the phosphorylation status of Akt, an indicator of PI3K Akt signaling, in DJ-1A RNAi animals. Head extracts from *Da-GAL4* and *Da-GAL4 DJ-1A RNAi* animals were analyzed by Western blot analysis by using anti-phospho-Akt and anti-Akt antibodies. As shown in Fig. 5*B*, although the level of total Akt protein was comparable between control and DJ-1A RNAi fly heads, the amount of phospho-Akt was significantly reduced in *DJ-1A RNAi* animals. This result indicates that DJ-1A down-regulation leads to hypophosphorylation of Akt and impairment of PI3K Akt signaling in the fly brain. To test whether impairment of PI3 Akt signaling is a general feature of PD models, we analyzed the *Drosophila parkin* model. As shown in Fig. 5*C*, inhibition of Parkin function also led to a reduction of phospho-Akt levels. These results implicate reduced PI3K Akt signaling as a common molecular event in the pathogenic cascade of PD.

Discussion

Loss-of-function mutations in human DJ-1 are linked to familial Parkinson's disease. The exact molecular function of DJ-1 that is relevant to disease pathogenesis is not well understood. Our results suggest that *Drosophila* DJ-1A plays an important role in cellular ROS homeostasis and protection against oxidative stress. This conclusion is consistent with previous studies in mammalian cell culture and DJ-1 knockout mice (13, 27, 30). Human DJ-1 was found to have H_2O_2-scavenging activity *in vitro*. (10) (27). Our analysis of *Drosophila* DJ-1A protein supported this notion. However, the H_2O_2-converting activity of DJ-1A is rather low compared with catalase, suggesting that the main molecular function of DJ-1 may not be limited to degrading H_2O_2. It is possible that the ability

nature neuroscience

Chromogranin-mediated secretion of mutant superoxide dismutase proteins linked to amyotrophic lateral sclerosis

Makoto Urushitani[1], Attila Sik[2], Takashi Sakurai[3], Nobuyuki Nukina[3], Ryosuke Takahashi[4] & Jean-Pierre Julien[1]

Here we report that chromogranins, components of neurosecretory vesicles, interact with mutant forms of superoxide dismutase (SOD1) that are linked to amyotrophic lateral sclerosis (ALS), but not with wild-type SOD1. This interaction was confirmed by yeast two-hybrid screen and by co-immunoprecipitation assays using either lysates from Neuro2a cells coexpressing chromogranins and SOD1 mutants or lysates from spinal cord of ALS mice. Confocal and immunoelectron microscopy revealed a partial colocalization of mutant SOD1 with chromogranins in spinal cord of ALS mice. Mutant SOD1 was also found in immuno-isolated trans-Golgi network and in microsome preparations, suggesting that it can be secreted. Indeed we report evidence that chromogranins may act as chaperone-like proteins to promote secretion of SOD1 mutants. From these results, and our finding that extracellular mutant SOD1 can trigger microgliosis and neuronal death, we propose a new ALS pathogenic model based on the toxicity of secreted SOD1 mutants.

ALS is a progressive adult-onset neurodegenerative disorder that affects primarily motor neurons in the brain and spinal cord. The disease typically begins locally and spreads, leading to paralysis and death within 3–5 years. Approximately 10% of ALS cases are familial and 90% are sporadic. Mutations in the genes encoding SOD1 (ref. 1) are involved in 20% of familial ALS cases.

Despite a decade of investigation on familial ALS caused by missense mutations in the *SOD1* gene, the mechanism of toxicity to motor neurons has remained elusive. Transgenic mice expressing mutant forms of SOD1 develop motor neuron disease resembling ALS through a gain of unidentified deleterious properties[2]. Eliminating the copper chaperone for SOD1 does not diminish the toxicity of mutant SOD1 in mice[3], and mutations that disrupt the copper-binding site of mutant SOD1 do not suppress toxicity[4]. Thus, it is now thought that the toxicity of mutant SOD1 is not related to aberrant copper-mediated catalysis but rather to the propensity of the abnormal protein to aggregate, a phenomenon common to many neurodegenerative diseases[5,6]. Cell culture studies have shown that the mutant SOD1 proteins induce oxidative stress[7,8], form aggregates[9,10] and impair proteasomal function[11].

Notably, recent lines of evidence indicate that the toxicity of SOD1 mutants is non-cell-autonomous. The neuron-specific expression of mutant SOD1 does not provoke motor neuron disease[12,13]. Moreover, chimeric mouse studies with SOD1 mutants have demonstrated that neurodegeneration is delayed or eliminated when motor neurons expressing mutant SOD1 are surrounded by healthy wild-type cells[14]. Moreover, these studies show evidence of damage to wild-type motor neurons by surrounding cells expressing mutant SOD1. Such results emphasize the importance of a motor neuron milieu, but the mechanism by which the toxicity of mutant SOD1 may be transferred from one cell to another is still unclear[14].

So far, proteins known to interact with mutant forms of SOD1 but not with wild-type SOD1 have been implicated in protein refolding or proteasomal degradation (for example, heat-shock proteins Hsp40, Hsp/Hsc70 (refs. 15,16) and CHIP[16]). To search for more proteins that interact with mutant SOD1, we performed yeast two-hybrid screening of a cDNA library from the total spinal cord of presymptomatic transgenic mice expressing the G93A SOD1 mutation (in which a glycine residue is replaced by an alanine residue). We discovered that chromogranins are interacting partners with mutant forms of SOD1, but not wild-type SOD1. The chromogranins, namely chromogranin-A (CgA) and chromogranin-B (CgB), are soluble, acidic glycophosphoproteins and are major constituents of secretory large dense-core vesicles (LDCV) in neurons and endocrine cells. LDCV store neuropeptides and hormones and show regulated exocytosis upon appropriate cellular stimulation[17]. Chromogranins are transported in the trans-Golgi network (TGN) and translocate at the periphery in an actin-dependent manner during their maturation process[18]. Although the physiological functions of chromogranins are still unclear, previous reports have shown that their proteolytic products function as antibiotics, regulators of hormone release, controllers of intracellular Ca^{2+} concentration and protein sorting machineries[17]. The role of chromogranins in neurons is unknown. Both CgA and CgB proteins are transported in the rat sciatic

[1]Department of Anatomy and Physiology, Laval University, Centre de Recherche du Centre Hospitalier de l' Université Laval, 2705 boulevard Laurier, Sainte-Foy, Quebec G1V 4G2, Canada. [2]Department of Psychiatry, Centre de Recherche Université Laval Robert-Giffard, 2601 de la Canardiere, Quebec, Quebec G1J 2G3, Canada. [3]Laboratory for Structural Neuropathology and [4]Motor System Neurodegeneration, RIKEN Brain Science Institute, 2-1 Hirosawa, Wako, Saitama, 351-0198, Japan. Correspondence should be addressed to J.-P.J. (jean-pierre.julien@crchul.ulaval.ca).

Received 15 September; accepted 26 October; published online 20 December 2005; doi:10.1038/nn1603

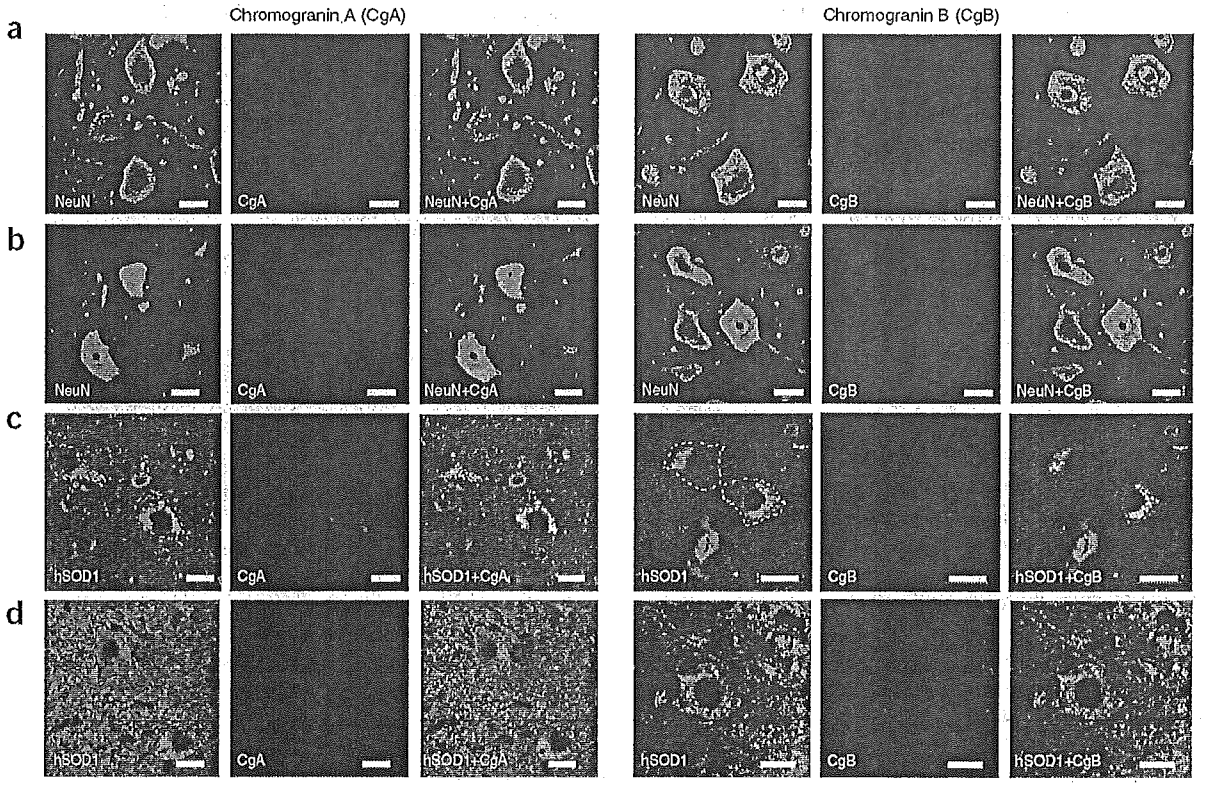

Figure 2 Expression pattern of chromogranins in *SOD1* transgenic mice. We used the lumbar spinal cords from **(a)** nontransgenic littermates, **(b,c)** transgenic mice at 7 months of age and **(d)** transgenic mice at 9 months of age. The transgenic mice expressed either G37R *SOD1* **(b,c)** or wild-type *SOD1* **(d)**. The following combinations of antibody stains were used: **(a,b)** mouse monoclonal anti-NeuN plus rabbit polyclonal anti-CgA (left) or anti-CgB (right); **(c,d)** sheep polyclonal antibody specific to human SOD1 plus anti-CgA (left) or anti-CgB (right). In **c**, the dotted lines demarcate the cell body of motor neurons. Scale bars, 50 μm.

promote secretion of misfolded SOD1 mutants. Moreover, our results demonstrate that extracellular mutant SOD1 can induce microgliosis and motor neuron death, suggesting that the chromogranin-mediated secretion of mutant SOD1 proteins could be a pathogenic mechanism in ALS. This idea is consistent with findings that the disease is not strictly autonomous to motor neurons and that toxicity is transferable from one cell to another.

RESULTS

Interaction of CgA and CgB with mutant SOD1 in cultured cells

To identify new proteins that interact with mutant SOD1, we used a yeast two-hybrid approach to screen a cDNA library from the spinal cord of pre-symptomatic mice transgenic for human G93A *SOD1*, using monomeric LexA-human G93A SOD1 as bait. As expected, the majority of the 250 surviving clones expressed human SOD1 that can dimerize with the bait. However, we obtained one clone whose sequence corresponded to a partial mouse CgB sequence encoding 76 amino acids. A full-length mouse CgB clone was then isolated from a brain cDNA library of C57Bl/6 mice and used as bait in the yeast two-hybrid system to confirm a specific interaction of CgB with mutant SOD1, but not with wild-type SOD1 (data not shown). To further investigate the interaction of CgB with mutant forms of SOD1 in a mammalian cell system, we carried out transient coexpression assays with Neuro2a cells using plasmid vectors coding for CgB tagged with hemagglutinin (HA) at the carboxy (C) terminus and for various human SOD1 species tagged with FLAG at the amino (N) terminus. We tested various SOD1 mutants, including the A4V, G85R and G93A mutants, to confirm that chromogranins interact with misfolded SOD1 mutants in general, not just the G93A mutant. As shown in pull-down assays (**Fig. 1a**), CgB was co-immunoprecipitated with mutant forms of SOD1, but not with wild-type SOD1. Pull-down assays revealed that CgA, another member of the mouse chromogranin family, also associated with SOD1 mutants but not with wild-type SOD1 (**Fig. 1b**). Similar results were obtained with human chromogranins (data not shown).

CgA and CgB share two conserved domains near their N and C termini, named the granin domains. The N-terminal granin domain is implicated in a sorting mechanism[27], whereas the C-terminal granin domain is necessary for dimerization or tetramerization of chromogranins[28]. To determine the CgB region responsible for interaction with mutant SOD1, we constructed expression plasmids for CgB mutants lacking specific domains and transiently expressed them together with mutant SOD1 into Neuro2a cells (**Fig. 1c**, top). An immunoprecipitation experiment showed that CgB mutants with deleted granin domains (ΔN or ΔC) were still able to interact with mutant SOD1 (**Fig. 1c**, bottom). A search for sequence homologies revealed that both CgB and CgA contain internal sequences with homologies to the substrate-binding site of mammalian Hsp70 (**Supplementary Fig. 1** online). A CgB mutant lacking this internal region (ΔHsp) did not bind mutant SOD1, as determined by the pull-down assay (**Fig. 1c**). The presence of an Hsp70-like domain offers a reasonable explanation for the specific binding of chromogranins to misfolded SOD1 mutants and not to wild-type SOD1.

Confocal microscopy of transfected Neuro2a cells provided further evidence of interactions between SOD1 mutants and chromogranins. Transfection of a construct encoding CgB fused at the C terminus to

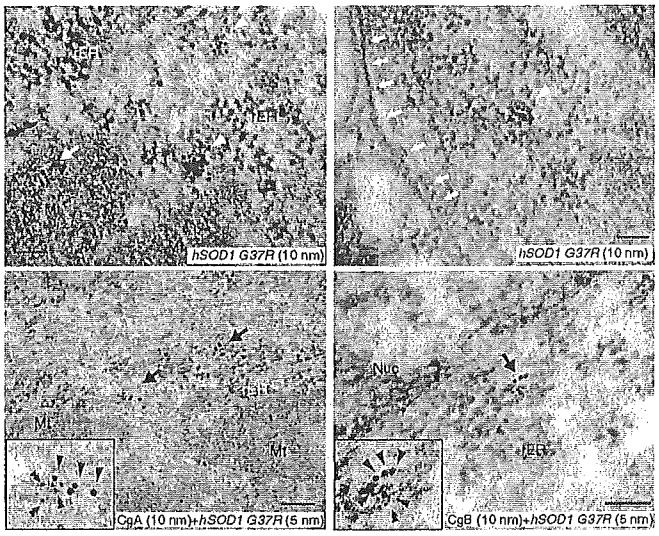

Figure 4 Immunoelectron microscopy reveals partial colocalization of G37R SOD1 with chromogranins. Ultra-thin sections of spinal anterior horn from G37R *SOD1* mice (7 months old) were incubated with sheep polyclonal antibody to human SOD1 alone (top panels), or together with rabbit polyclonal antibody to CgA or CgB (lower left or right, respectively). For secondary antibody, we used 10-nm (top panels) or 5-nm (bottom panels) immunogold-conjugated anti-sheep IgG and 10-nm immunogold-conjugated anti-rabbit IgG antibodies. In rough ER, 10-nm clusters of immuno-gold particles were frequently detected (arrowheads). G37R SOD1 was occasionally detected in mitochondria (arrow, top-left), or in a vesicle (arrowhead, top-right) close to the plasma membrane (arrows, top-right). Double-staining revealed frequent 10-nm clusters of CgA or CgB (arrowheads, bottom left or right) and 5-nm gold particles (hSOD1, double arrowheads, bottom panels). Scale bars, 100 nm.

fractions, whereas only 2.61% of wild-type SOD1 accumulated there (**Fig. 3a**, bottom). Furthermore, G37R SOD1 but not wild-type SOD1 formed non-native dimers and high molecular aggregates in the membrane fractions in an age-dependent manner. To further clarify the distribution of mutant SOD1 in the transport vesicles, we performed sucrose density gradient ultracentrifugation of post-mitochondrial membrane fractions using spinal cord extract from presymptomatic G37R *SOD1* transgenic mice at 7 months old. Western blotting revealed that mutant SOD1 had a distribution pattern similar to chromogranins, the trans-Golgi marker adaptin-γ and the SNARE protein syntaxin-1, but different from the pattern of synaptophysin (**Fig. 3b**).

To further confirm the distribution of mutant SOD1 species in a secretory pathway, we purified TGN from the spinal cord lysates of *SOD1* (wild-type), G37R *SOD1* and G93A *SOD1* transgenic mice by an immuno-isolation technique using anti-TGN38 antibody bound to protein G–coated magnetic beads. Anti-TGN38 is an affinity-purified polyclonal antibody specific to a 23-amino acid peptide corresponding to the cytosolic domain of rat and mouse TGN38 protein. Western analysis of the immunoprecipitates demonstrated that both G37R and G93A SOD1 co-precipitated with TGN38, indicating that mutant SOD1 is distributed in the TGN (**Fig. 3c**). Note that the wild-type SOD1 was also detectable in the TGN preparation, albeit at lower levels than mutant SOD1.

Further evidence for the specific interaction of CgA or CgB with mutant SOD1 proteins came from co-immunoprecipitation experiments using spinal cord lysates of transgenic mice. We found that rabbit polyclonal anti-CgA or anti-CgB antibody was able to pull down both G37R and G93A SOD1 mutants but not wild-type SOD1 (**Fig. 3d**). It should be noted that a non-native dimer of G37R SOD1 was more apparent than G93A SOD1 (double arrowhead), corresponding to the larger amount of co-immunoprecipitated G37R SOD1 than G93A SOD1.

To further investigate the distribution and colocalization of mutant SOD1 and chromogranins, we examined spinal cord sections from *SOD1* (wild-type) and G37R *SOD1* transgenic mice (7 months old) using immunoelectron microscopy. Mutant SOD1 protein was observed as small clusters of gold particles in the cytosol (**Supplementary Fig. 3** online), rough ER (arrowheads in **Fig. 4**, top-left), smooth ER and Golgi (**Supplementary Fig. 3**), and occasionally it was observed in mitochondria (arrow in **Fig. 4**, top-left) and transport vesicles (**Fig. 4**, top-right). Moreover, the double immunohistochemistry using secondary antibodies conjugated with different gold particles (5 nm or 10 nm) provided frequent detection of cluster complexes

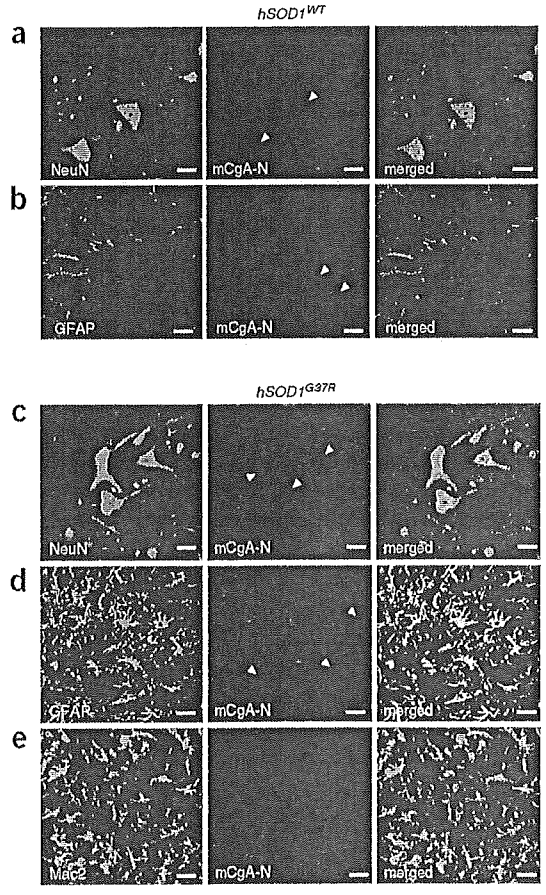

Figure 5 CgA is expressed in reactive astrocytes of spinal anterior horn from mutant *SOD1* transgenic mice. Double immunofluorescent experiments show the colocalization of CgA and GFAP in the spinal cord of transgenic mice carrying mutant *SOD1*, but not those carrying wild-type *SOD1*. (**a**,**b**) In wild-type *SOD1* mice, CgA was expressed only in the neurons labeled by anti-NeuN (**a**, mouse monoclonal), but not in reactive astrocytes labeled by anti-GFAP (**b**, mouse monoclonal). In G37R *SOD1* mice, in addition to the neuronal expression (**c**), CgA was also detected in reactive astrocytes (**d**), but not in the active microglial cells labeled by anti-Mac2 (**e**, rat monoclonal). Arrowheads and arrows, respectively, indicate neurons and astrocytes stained with anti-mCgA-N′. Left panels represent merged images from left and middle panels. Scale bars, 50 μm. Images show a representative sample from one of at least three independent experiments.

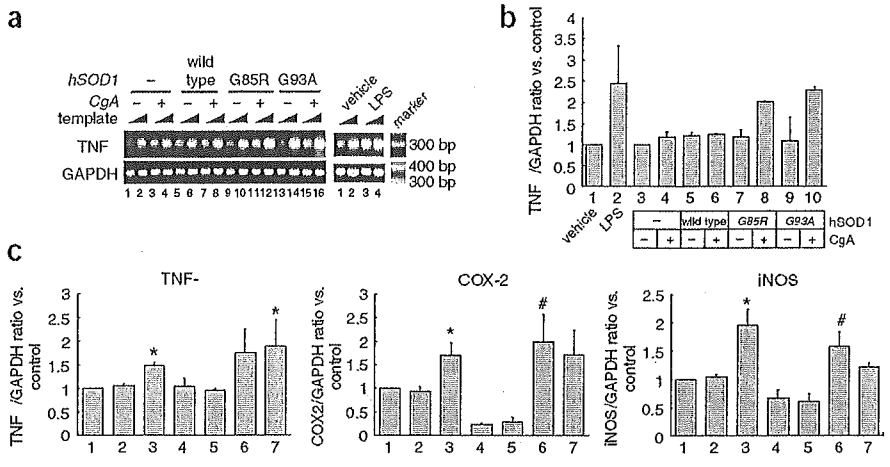

Figure 7 Activation of microglia by extracellular mutant SOD1. (**a**,**b**) Activation of microglial cell-line BV2 after treatment with conditioned medium from Neuro2a cells co-transfected with CgA and *SOD1* mutants (G85R or G93A). (**a**) RT-PCR study of TNF-α and GAPDH. For control, Neuro2a cells were treated with lipopolysaccharide (LPS). Notably, there was no microglial activation with medium from cells co-transfected with *CgA* and wild-type *SOD1*. Templates were examined at two different concentrations (1:10 diluted and original). (**b**) Each densitometric value was normalized with GAPDH and averaged from results of two different concentrations of templates. Each value represents a ratio compared to control lanes (bar 1 is the control for bar 2, and bar 3 is the control for 4–10), expressed as mean ± s.e.m. (**c**) Direct effect of mutant SOD1 on microglial activation. BV2 cells were treated with recombinant CgA (1 μg ml $^{-1}$), human SOD1 (wild-type or G93A, 2 μg ml $^{-1}$ each) or LPS (10 μg ml $^{-1}$) as a positive control for 18 h, as shown in the bottom box. Semi-quantitative RT-PCR was performed in the same manner as in **a**. Each densitometric value was normalized by GAPDH and an expression ratio was obtained by comparison with control (bar 1 in each graph). The ratio was averaged from three experiments and expressed as mean ± s.e.m. $^{*}P < 0.05$ versus sham treatment (lane 1). $^{\#}P < 0.05$ versus wild-type SOD1 treatment (lane 4) assessed by analysis of variance (ANOVA).

mutant SOD1 with chromogranins in mouse models of ALS. These results prompted us to investigate whether mutant SOD1 molecules were secreted together with chromogranins. We conducted secretion experiments using nongranular COS-7 cells that are lacking endogenous chromogranins[33]. Expression plasmids coding for FLAG-tagged SOD1 (wild-type or G93A mutant) and HA-tagged mouse CgA or CgB were transiently co-transfected in COS-7 cells. Both wild-type and G93A mutant SOD1 were detected by western analysis in the control medium after a 15-min incubation. Moreover, treatment with stimulation buffer containing 2-mM $BaCl_2$ and 50 mM KCl increased the amount of both wild-type and mutant SOD1 in the medium 1.2-fold compared with control buffer (data not shown). These data imply the existence of constitutive and regulatory secretory pathways for SOD1 in these cells. It is noteworthy that both CgA and CgB promoted secretion of G93A SOD1, whereas secretion of wild-type SOD1 was not affected by CgA or CgB (**Fig. 6a,b**). Judging from the amount of lactate dehydrogenase (LDH) released, the effects of chromogranins on secretion of mutant SOD1 did not result from cell death or membrane disintegration caused by overexpression (**Fig. 6c**). We also examined the effect of Brefeldin A (BFA) on SOD1 secretion to further address the involvement of the ER-Golgi network. In COS-7 cells, BFA did not reduce the secretion of either mutant or wild-type SOD1 in absence of CgB (**Fig. 6d**, lanes 2 and 5). BFA did, however, inhibit the CgB-mediated secretion of mutant SOD1 (**Fig. 6d**, lanes 7 and 8). This suggests that CgB contributes to the secretion of mutant SOD1 proteins through the TGN. We conclude that chromogranins promote the secretion of mutant SOD1, but not of wild-type SOD1.

Proteasome inhibition enhances secretion of mutant SOD1

Because previous studies showed an impairment of proteasomal activity in cells expressing mutant SOD1[11], we examined the effect of a proteasome inhibitor on the secretion of human SOD1 species in non-granular NIH3T3 cells. The treatment of transfected NIH3T3 cells with a specific proteasome inhibitor, lactacystin (5 μM), enhanced the secretion of mutant SOD1 in the presence or absence of chromogranins (**Fig. 6e**).

SOD1 secretion from spinal cultures of SOD1 mouse embryo

Both wild-type and mutant SOD1 have been detected in the cerebrospinal fluid (CSF) of *SOD1* transgenic rats[34] and humans carrying a SOD1 mutation[35]. However, it is technically difficult to prove this finding in mice, because of the small space for CSF with high occurrence of contamination from the blood or tissues. We carried out spinal cord cultures from *SOD1* transgenic mice to confirm that SOD1 can be secreted. Spinal cord cultures were prepared from E13 embryos and then analyzed after 14 d *in vitro*. Secretion analysis of the culture medium revealed that both wild-type and G37R SOD1 can be detected in basal secretion buffer. Exposure of the cells to stimulation buffer containing $BaCl_2$ (2 mM) and KCl (50 mM) for 15 min promoted the secretion of both wild-type and G37R SOD1, but more robustly in G37R (**Fig. 6f**). This result indicates that SOD1 can be secreted in both a constitutive and regulated manner.

Extracellular SOD1 mutants cause microgliosis and neuron death

There is evidence for involvement of CgA in microglial activation[32]. To examine the effects of secreted mutant SOD1 together with CgA on microglial activation, we treated BV2 microglial cells with conditioned medium from Neuro2a cells that were transfected with various human *SOD1* species (wild-type, G85R and G93A), with or without CgA. Semi-quantitative reverse-transcriptase PCR (RT-PCR) was performed using total RNA from BV2 cells to monitor expression of mRNA for proinflammatory molecules. RT-PCR results showed that the combination of mutant SOD1 and CgA resulted in a medium that induced TNF-α expression in BV2 cells (**Fig. 7a,b**).

To investigate whether extracellular SOD1 mutants activate microglia, we exposed the BV2 cells to recombinant human SOD1 or CgA (extracellular) to determine whether microglial activation was mediated directly by these molecules. The results showed that extracellular mutant G93A SOD1 with or without CgA induced BV2 cells to produce TNF-α, cyclooxygenase-2 (COX-2) and inducible nitric oxide synthase (iNOS) (**Fig. 7c**). In contrast to mutant SOD1, the recombinant wild-type SOD1 caused suppression of microglial activation, which is in agreement with a protective role for secreted wild-type SOD1 as recently suggested[35].

We further investigated the effects of extracellular SOD1 (wild-type and G93A) and CgA proteins using primary spinal cord cultures derived from E13 mouse embryos. Spinal cord cultures at 14 d after plating were exposed to these recombinant proteins or to lipopolysaccharide (LPS) for 24 h. Treatment of the cultures with CgA and/or

trigger microgliosis and neuronal death and (v) CgA expression is induced in reactive astrocytes.

It is unclear how the mutant SOD1 proteins are being recruited in the ER-Golgi secretory granule pathway to interact with chromogranins. SOD1 protein has no signal sequence. It is possible that an increased hydrophobicity of mutant SOD1 underlies its translocation in the ER-Golgi pathway, as reported for fibroblast growth factor-16 (ref. 37). The cytosolic soluble protein SOD1 normally maintains its hydrophilicity through intramolecular disulfide bonds. However, mutant SOD1 proteins are readily monomerized by a reducing environment[38], resulting in exposure of hydrophobic regions that can be recognized by Hsp proteins[16]. Once recruited into the ER-Golgi system, it is plausible that oxidative conditions might promote the formation of oligomers, as detected in **Figure 3a**. Our findings are consistent with a previous report that mutant SOD1, but not wild-type SOD1, can induce ER stress when transfected into COS-7 cells, with accumulation of mutant SOD1 in or on the ER[39]. Although we cannot exclude the possibility of a gain of toxic function due to ER stress, our data demonstrate that secretion of mutant SOD1 may represent a toxic pathway which would be in line with the non-cell-autonomous nature of ALS[14].

It is still unclear how mutant SOD1 associates with chromogranins in the ER-Golgi network. The results from our yeast two-hybrid interaction studies support a direct association. Moreover, *in vitro* binding of recombinant CgA with mutant SOD1, but not with wild-type SOD1, was also confirmed (data not shown). The presence of Hsp70-like motifs in both CgB and CgA may explain why chromogranins interact with mutant forms of SOD1, but not with wild-type SOD1. Mutant SOD1 proteins are known to show altered solubility and interact with heat shock/stress proteins[15,16].

Previous studies have shown that wild-type SOD1 can be secreted from cultured astrocytes[40] or thymus-derived cells[41]. Moreover, it has been reported that both wild-type and mutant SOD1 species are detected in the cerebrospinal fluid of both transgenic rats[34] carrying human SOD1 and ALS patients with the SOD1 mutation[35]. Our data together with these observations support the idea that both wild-type and mutant SOD1 proteins may be secreted through non-classical secretory pathways[42]. In addition, we propose a chaperone-like function for chromogranins in mediating the selective secretion of misfolded SOD1 mutants through the ER-Golgi network. In a recent study[35] with NSC34 cells, the secretion was interpreted as being beneficial because the extrusion of mutant SOD1 attenuated formation of toxic intracellular inclusions, ameliorating cell survival. That study did not, however, consider the presence of glial cells in motor neuron environment *in vivo* or the possibility that the disease in not strictly cell autonomous[14]. Conversely, we posit that secretion of mutant SOD1 mediated by chromogranins is deleterious because extracellular mutant SOD1 proteins caused microgliosis and death of embryonic motor neurons in mixed cultures (**Fig. 8**). Unlike secreted mutant SOD1, extracellular wild-type SOD1 probably has protective properties. Our data suggest that extracellular wild-type SOD1 suppresses extracellular inflammation, perhaps through an antioxidant effect (**Fig. 7c**), which would be consistent with the finding that intraspinal infusion of exogenous wild-type SOD1 in G93A SOD1 transgenic rats prolonged their lifespan[34].

From our *in situ* hybridization data and immunohistochemistry of spinal cord samples, it seems that chromogranin expression is elevated in both motor neurons and interneurons (**Supplementary Fig. 2**). Therefore, as depicted in our proposed pathogenic scheme (**Supplementary Fig. 6**), we view interneurons as important contributors to the secretion of chromogranins and mutant SOD1 complexes in the vicinity of motor neurons. In this model, it is the burden of extracellular mutant SOD1 in close proximity to motor neurons that would increase the risk of damage. Even though interneurons and motor neurons themselves would be the predominant source of extracellular mutant SOD1 mediated by chromogranin interactions, mutant SOD1 secreted by other pathways from other cells such as microglia and astrocytes could also contribute to pathogenesis. Though the deleterious effects of intracellular mutant SOD1 can not be excluded, our model of toxicity based on secreted mutant SOD1 is compatible with the idea that the disease is not autonomous to motor neurons[14].

Although the exact mechanisms underlying the microgliosis and neurotoxicity of extracellular mutant SOD1 remain to be elucidated, various deleterious effects of misfolded SOD1 proteins may occur through generation of hydroxyl radicals[7], toxic oligomers[11] or amyloid-like filaments[43]. This model would support a linkage between inflammation and ALS pathogenesis[44,45]. Many factors may contribute to motor neuron death in the context of inflammation. Proinflammatory molecules such as TNF-α, Fas ligand or nitric oxide may act as mediators of motor neuron death[8]. Microglial activation alone is not usually sufficient to induce motor neuron death. For instance, induction of innate immunity by intraperitoneal injection of LPS does not injure motor neurons[44]. Chronic LPS administration precipitated ALS in mice, however, supporting the view that chronic inflammation may constitute a risk factor[44]. Yet, our data demonstrate that elimination of microglia by LLME did not alter survival of motor neurons and that LPS is much less toxic to motor neurons than mutant SOD1 in mixed embryonic spinal cord cultures (**Fig. 8b,e**). It is noteworthy that mutant SOD1, and to some extent wild-type SOD1, can be converted to toxic species even in absence of copper and zinc (**Fig. 8c**). This concurs with previous reports about the misfolded nature of apo-state SOD1 (refs. 16,43).

In conclusion, our results suggest a novel function for chromogranins in mediating the secretion of misfolded SOD1 mutants, a potentially toxic pathway that can induce inflammation and neuronal death. In future studies, it will be of interest to determine whether chromogranin-mediated secretion may be applicable to other neurodegenerative diseases that involve misfolded proteins.

METHODS

Materials. Commercially available antibodies are listed in **Supplementary Methods** online. The Golgi marker plasmid DsRed-Golgi, which carries the Golgi-targeting sequence of the human gene encoding β1,4-galactosyl transferase, was a generous gift from Y. Imai (RIKEN Brain Science Institute).

To generate an antibody specific to the N′ terminus of mouse CgA, we immunized rabbits with the peptide CLPVNSPMTKGDTKVMK, which encodes the amino terminal residues of mature mouse CgA (amino acids 18–35). The antisera were purified with an affinity column coupled with the same antigen. The titer and specificity were investigated by western blotting (**Supplementary Fig. 4**).

The recombinant proteins of human SOD1 (wild-type and mutant) and mouse CgA were generated from *Escherichia coli* as described in **Supplementary Methods**.

Transgenic mice. Transgenic mice harboring the G93A mutant of human *SOD1* (*B6SJL-TgN[SOD1-G93A]^{dl}1Gur, B6SJL-TgN[SOD1-G93A]1Gur*) and those harboring wild-type human *SOD1* (*C57Bl/6-TgN[SOD1]3Cje, hSOD1^{WT}*) were purchased from The Jackson Laboratory. Transgenic mice carrying G37R *SOD1* (line 29) were a kind gift from D. Cleveland (University of California, San Diego) and were housed and bred with C57Bl/6 mice. We selected these mouse lines because they were readily available to us. Since we maintain a larger colony of G37R *SOD1* (line 29) mice, most of our experiments involving mouse analysis were done with this line. Mice were treated with 10% chloral hydrate for anesthesia before they were perfused or killed. Animals were handled in accordance with the approved protocol by the animal experiment committees at RIKEN Brain Science Institute and by the Comité de Protection des Animaux de l'Université Laval.

cultures were treated at 11 or 14 d after plating. Motor neurons were identified as large cells labeled with SMI32 and active microglia were detected with Mac2-specific antibody. Confocal microscopy images were obtained from eight randomly selected fields, and immunoreactive cells were counted by computer. In several experiments, microglia were eliminated by a 16-h treatment with LLME[36] before exposure to recombinant SOD1 proteins. In preliminary experiments, we noticed that 5-mM LLME for 16 h killed approximately 60–70% of Mac2-positive cells. The number of cells was calculated as cells per mm^2 and averaged. Statistical significance was evaluated by single-factor ANOVA (analysis of variance) following Scheffe's method.

Note: Supplementary information is available on the Nature Neuroscience website.

ACKNOWLEDGMENTS

We thank R. Janvier for sample preparation for immunoelectron microscopy and B. Gentil for advice on experimental procedures. The technical help from G. Soucy, S.A. Ezzi (Laval University) and J. Kurisu (RIKEN Brain Science Institute) is appreciated. We thank D. Cleveland (University of California San Diego) for the G37R *SOD1* transgenic mice and Y. Imai for the *DsRed-Golgi* plasmid. This work was supported by the Canadian Institutes of Health Research (CIHR), the Robert Packard Centre for ALS Research at Johns Hopkins, the ALS Association (USA), the ALS Society of Canada, the Japan Society for the Promotion of Science (JSPS) and the Japan Foundation for Neuroscience and Mental Health. J.-P.J. holds a Canada Research Chair in Neurodegeneration. M.U. is a recipient of a Uehara Memorial Foundation research fellowship and a postdoctoral fellowship from CIHR.

COMPETING INTERESTS STATEMENT

The authors declare that they have no competing financial interests.

Published online at http://www.nature.com/natureneuroscience/
Reprints and permissions information is available online at http://npg.nature.com/reprintsandpermissions/

1. Rosen, D.R. *et al.* Mutations in Cu/Zn superoxide dismutase gene are associated with familial amyotrophic lateral sclerosis. *Nature* **362**, 59–62 (1993).
2. Gurney, M.E. *et al.* Motor neuron degeneration in mice that express a human Cu,Zn superoxide dismutase mutation. *Science* **264**, 1772–1775 (1994).
3. Subramaniam, J.R. *et al.* Mutant SOD1 causes motor neuron disease independent of copper chaperone-mediated copper loading. *Nat. Neurosci.* **5**, 301–307 (2002).
4. Wang, J., Xu, G. & Borchelt, D.R. High molecular weight complexes of mutant superoxide dismutase 1: age-dependent and tissue-specific accumulation. *Neurobiol. Dis.* **9**, 139–148 (2002).
5. Julien, J.P. Amyotrophic lateral sclerosis. unfolding the toxicity of the misfolded. *Cell* **104**, 581–591 (2001).
6. Cleveland, D.W. & Rothstein, J.D. From Charcot to Lou Gehrig: deciphering selective motor neuron death in ALS. *Nat. Rev. Neurosci.* **2**, 806–819 (2001).
7. Wiedau-Pazos, M. *et al.* Altered reactivity of superoxide dismutase in familial amyotrophic lateral sclerosis. *Science* **271**, 515–518 (1996).
8. Raoul, C. *et al.* Motoneuron death triggered by a specific pathway downstream of Fas: potentiation by ALS-linked SOD1 mutations. *Neuron* **35**, 1067–1083 (2002).
9. Durham, H.D., Roy, J., Dong, L. & Figlewicz, D.A. Aggregation of mutant Cu/Zn superoxide dismutase proteins in a culture model of ALS. *J. Neuropathol. Exp. Neurol.* **56**, 523–530 (1997).
10. Johnston, J.A., Dalton, M.J., Gurney, M.E. & Kopito, R.R. Formation of high molecular weight complexes of mutant Cu, Zn-superoxide dismutase in a mouse model for familial amyotrophic lateral sclerosis. *Proc. Natl. Acad. Sci. USA* **97**, 12571–12576 (2000).
11. Urushitani, M., Kurisu, J., Tsukita, K. & Takahashi, R. Proteasomal inhibition by misfolded mutant superoxide dismutase 1 induces selective motor neuron death in familial amyotrophic lateral sclerosis. *J. Neurochem.* **83**, 1030–1042 (2002).
12. Pramatarova, A., Laganière, J., Roussel, J., Brisebois, K. & Rouleau, G.A. Neuron-specific expression of mutant superoxide dismutase 1 in transgenic mice does not lead to motor impairment. *J. Neurosci.* **21**, 3369–3374 (2001).
13. Lino, M.M., Schneider, C. & Caroni, P. Accumulation of SOD1 mutants in postnatal motoneurons does not cause motoneuron pathology or motoneuron disease. *J. Neurosci.* **22**, 4825–4832 (2002).
14. Clement, A.M. *et al.* Wild-type nonneuronal cells extend survival of SOD1 mutant motor neurons in ALS mice. *Science* **302**, 113–117 (2003).
15. Shinder, G.A., Lacourse, M.C., Minotti, S. & Durham, H.D. Mutant Cu/Zn-superoxide dismutase proteins have altered solubility and interact with heat shock/stress proteins in models of amyotrophic lateral sclerosis. *J. Biol. Chem.* **276**, 12791–12796 (2001).
16. Urushitani, M. *et al.* CHIP promotes proteasomal degradation of familial ALS-linked mutant SOD1 by ubiquitinating Hsp/Hsc70. *J. Neurochem.* **90**, 231–244 (2004).
17. Taupenot, L., Harper, K.L. & O'Connor, D.T. The chromogranin-secretogranin family. *N. Engl. J. Med.* **348**, 1134–1149 (2003).
18. Rudolf, R., Salm, T., Rustom, A. & Gerdes, H.H. Dynamics of immature secretory granules: role of cytoskeletal elements during transport, cortical restriction, and f-actin-dependent tethering. *Mol. Biol. Cell* **12**, 1353–1365 (2001).
19. Li, J.Y., Leitner, B., Lovisetti-Scamihorn, P., Winkler, H. & Dahlström, A. Proteolytic processing, axonal transport and differential distribution of chromogranins A and B, and secretogranin II (secretoneurin) in rat sciatic nerve and spinal cord. *Eur. J. Neurosci.* **11**, 528–544 (1999).
20. Booj, S., Goldstein, M., Fischer-Colbrie, R. & Dahlstrom, A. Calcitonin gene-related peptide and chromogranin A: presence and intra-axonal transport in lumbar motor neurons in the rat, a comparison with synaptic vesicle antigens in immunohistochemical studies. *Neuroscience* **30**, 479–501 (1989).
21. Marksteiner, J. *et al.* Distribution of chromogranin B-like immunoreactivity in the human hippocampus and its changes in Alzheimer's disease. *Acta Neuropathol. (Berl.)* **100**, 205–212 (2000).
22. Rangon, C.M. *et al.* Different chromogranin immunoreactivity between prion and a-beta amyloid plaque. *Neuroreport* **14**, 755–758 (2003).
23. Schiffer, D., Cordera, S., Giordana, M.T., Attanasio, A. & Pezzulo, T. Synaptic vesicle proteins, synaptophysin and chromogranin A in amyotrophic lateral sclerosis. *J. Neurol. Sci.* **129** Suppl, 68–74 (1995).
24. Taupenot, L. *et al.* Chromogranin A triggers a phenotypic transformation and the generation of nitric oxide in brain microglial cells. *Neuroscience* **72**, 377–389 (1996).
25. Ciesielski-Treska, J. *et al.* Mechanisms underlying neuronal death induced by chromogranin A-activated microglia. *J. Biol. Chem.* **276**, 13113–13120 (2001).
26. Taylor, D.L., Diemel, L.T. & Pocock, J.M. Activation of microglial group III metabotropic glutamate receptors protects neurons against microglial neurotoxicity. *J. Neurosci.* **23**, 2150–2160 (2003).
27. Chanat, E., Weiss, U., Huttner, W.B. & Tooze, S.A. Reduction of the disulfide bond of chromogranin B (secretogranin I) in the trans-Golgi network causes its missorting to the constitutive secretory pathways. *EMBO J.* **12**, 2159–2168 (1993).
28. Cowley, D.J., Moore, Y.R., Darling, D.S., Joyce, P.B. & Gorr, S.U. N- and C-terminal domains direct cell type-specific sorting of chromogranin A to secretory granules. *J. Biol. Chem.* **275**, 7743–7748 (2000).
29. Li, J.Y., Kling-Petersen, A. & Dahlstrom, A. Influence of spinal cord transection on the presence and axonal transport of CGRP-, chromogranin A-, VIP-, synapsin I-, and synaptophysin-like immunoreactivities in rat motor nerve. *J. Neurobiol.* **23**, 1094–1110 (1992).
30. Kato, A. *et al.* Co-distribution patterns of chromogranin B-like immunoreactivity with chromogranin A and secretoneurin within the human brainstem. *Brain Res.* **852**, 444–452 (2000).
31. Stieber, A. *et al.* Disruption of the structure of the Golgi apparatus and the function of the secretory pathway by mutants G93A and G85R of Cu, Zn superoxide dismutase (SOD1) of familial amyotrophic lateral sclerosis. *J. Neurol. Sci.* **219**, 45–53 (2004).
32. Ciesielski-Treska, J. *et al.* Chromogranin A induces a neurotoxic phenotype in brain microglial cells. *J. Biol. Chem.* **273**, 14339–14346 (1998).
33. Huh, Y.H., Jeon, S.H. & Yoo, S.H. Chromogranin B-induced secretory granule biogenesis: comparison with the similar role of chromogranin A. *J. Biol. Chem.* **278**, 40581–40589 (2003).
34. Turner, B.J. *et al.* Impaired extracellular secretion of mutant superoxide dismutase 1 associates with neurotoxicity in familial amyotrophic lateral sclerosis. *J. Neurosci.* **25**, 108–117 (2005).
35. Jacobsson, J., Jonsson, P.A., Andersen, P.M., Forsgren, L. & Marklund, S.L. Superoxide dismutase in CSF from amyotrophic lateral sclerosis patients with and without CuZn-superoxide dismutase mutations. *Brain* **124**, 1461–1466 (2001).
36. Sharpless, N. *et al.* The restricted nature of HIV-1 tropism for cultured neural cells. *Virology* **191**, 813–825 (1992).
37. Miyakawa, K. & Imamura, T. Secretion of FGF-16 requires an uncleaved bipartite signal sequence. *J. Biol. Chem.* **278**, 35718–35724 (2003).
38. Tiwari, A. & Hayward, L.J. Familial amyotrophic lateral sclerosis mutants of copper/zinc superoxide dismutase are susceptible to disulfide reduction. *J. Biol. Chem.* **278**, 5984–5992 (2003).
39. Tobisawa, S. *et al.* Mutant SOD1 linked to familial amyotrophic lateral sclerosis, but not wild-type SOD1, induces ER stress in COS7 cells and transgenic mice. *Biochem. Biophys. Res. Commun.* **303**, 496–503 (2003).
40. Lafon-Cazal, M. *et al.* Proteomic analysis of astrocytic secretion in the mouse. Comparison with the cerebrospinal fluid proteome. *J. Biol. Chem.* **278**, 24438–24448 (2003).
41. Cimini, V. *et al.* CuZn-superoxide dismutase in human thymus: immunocytochemical localisation and secretion in thymus-derived epithelial and fibroblast cell lines. *Histochem. Cell Biol.* **118**, 163–169 (2002).
42. Nickel, W. The mystery of nonclassical protein secretion. A current view on cargo proteins and potential export routes. *Eur. J. Biochem.* **270**, 2109–2119 (2003).
43. Elam, J.S. *et al.* Amyloid-like filaments and water-filled nanotubes formed by SOD1 mutant proteins linked to familial ALS. *Nat. Struct. Biol.* **10**, 461–467 (2003).
44. Nguyen, M.D., D'Aigle, T., Gowing, G., Julien, J.P. & Rivest, S. Exacerbation of motor neuron disease by chronic stimulation of innate immunity in a mouse model of amyotrophic lateral sclerosis. *J. Neurosci.* **24**, 1340–1349 (2004).
45. Zhu, S. *et al.* Minocycline inhibits cytochrome c release and delays progression of amyotrophic lateral sclerosis in mice. *Nature* **417**, 74–78 (2002).
46. Parkin, E.T., Hussain, I., Karran, E.H., Turner, A.J. & Hooper, N.M. Characterization of detergent-insoluble complexes containing the familial Alzheimer's disease-associated presenilins. *J. Neurochem.* **72**, 1534–1543 (1999).
47. Stephens, D.J. & Banting, G. Direct interaction of the trans-Golgi network membrane protein, TGN38, with the F-actin binding protein, neurabin. *J. Biol. Chem.* **274**, 30080–30086 (1999).

The neuropeptide head activator is a high-affinity ligand for the orphan G-protein-coupled receptor GPR37

Meriem Rezgaoui[1], Ute Süsens[1], Atanas Ignatov[1], Mathias Gelderblom[2], Günter Glassmeier[3], Inga Franke[1], Jens Urny[1], Yuzuru Imai[4], Ryosuke Takahashi[4] and H. Chica Schaller[1,*]

[1]Zentrum für Molekulare Neurobiologie Hamburg, [2]Klinik und Poliklinik für Neurologie, and [3]Institut für Angewandte Physiologie, Universitätsklinikum Hamburg-Eppendorf, Martinistr. 52, 20246 Hamburg, Germany
[4]RIKEN Brain Science Institute, Saitama 351-0198, Japan
*Author for correspondence (e-mail: schaller@zmnh.uni-hamburg.de)

Accepted 26 October 2005
Journal of Cell Science 119, 542-549 Published by The Company of Biologists 2006
doi:10.1242/jcs.02766

Summary

The neuropeptide head activator (HA) is a mitogen for mammalian cell lines of neuronal or neuroendocrine origin. HA signalling is mediated by a G-protein-coupled receptor (GPCR). Orphan GPCRs with homology to peptide receptors were screened for HA interaction. Electrophysiological recordings in frog oocytes and in mammalian cell lines as well as Ca^{2+} mobilisation assays revealed nanomolar affinities of HA to GPR37. HA signal transduction through GPR37 was mediated by an inhibitory G protein and required Ca^{2+} influx through a channel of the transient receptor potential (TRP) family. It also required activation of Ca^{2+}-dependent calmodulin kinase and phosphoinositide 3-kinase. Respective inhibitors blocked HA signalling and HA-induced mitosis in GPR37-expressing cells. HA treatment resulted in internalisation of GPR37. Overexpression of GPR37 led to aggregate formation, retention of the receptor in the cytoplasm and low survival rates of transfected cells, confirming the notion that misfolded GPR37 contributes to cell death, as observed in Parkinson's disease.

Key words: G-protein-coupled receptor, GPR37, Head activator, Pael receptor, Parkinson, Signal transduction

Introduction

The undecapeptide head activator (HA) was originally isolated and characterised from hydra, where it mediates head-specific growth and differentiation processes, hence its name. In hydra, HA is produced by nerve cells and is stored in neurosecretory granules, from which it is released to initiate head regeneration and budding, and to maintain the normal head-to-foot morphology of hydra. At the cellular level, HA promotes proliferation of all cell types of hydra by acting as mitogen in the G2-mitosis transition; as for early mammalian development, this transition is the most important checkpoint to control cell-cycle progression. At higher concentrations, HA acts on the determination of stem cells to head-specific fates (Schaller et al., 1996).

HA was isolated with identical sequence from mammalian brain and intestine (Bodenmuller and Schaller, 1981). In adult mammals, HA enhances neurite outgrowth and is neuroprotective. HA is present during early mammalian development and is expressed in cells of the nervous and neuroendocrine system. Like in hydra, HA stimulates entry into mitosis and proliferation of cell lines derived from such origins. The signalling cascade from HA to mitosis includes activation of an inhibitory G protein and requires Ca^{2+} influx, downregulation of adenylyl cyclase and hyperpolarisation of the membrane potential (Kayser et al., 1998; Niemann and Schaller, 1996; Ulrich et al., 1996). For Ca^{2+} influx, a transient receptor potential (TRP)-like channel is responsible, which can be regulated by growth factors, such as insulin growth factor I (IGF-I) and platelet-derived growth factor (PDGF) (Kanzaki et al., 1999), and by HA (Boels et al., 2001). The increase in intracellular Ca^{2+} then triggers influx of K^+ through a Ca^{2+}-activated K^+ channel, leading to hyperpolarisation, which is an absolute requirement for entry into mitosis (Kayser et al., 1998).

In the search for receptors mediating the action of HA on stimulating mitosis in mammalian cells, we concentrated on orphan G-protein-coupled receptors (GPCRs) reacting with small peptides as ligands. GPCRs are the largest family of cell-surface receptors that mediate transduction of signals from the extracellular environment to intracellular effectors. They contain seven transmembrane domains and are activated by ligands of extremely different molecular origins and sizes including light, ions, metabolic intermediates, amino acids, nucleotides, lipids, peptides and proteins. These ligands primarily interact with the extracellular domains, but in part also with transmembrane regions of GPCRs. The classification of GPCRs into subfamilies is primarily based on their homology within the heptahelical structure (Frederiksson et al., 2003), but also on extracellular domains, and has been used to predict ligands for orphan receptors (Boels and Schaller, 2003; Ignatov et al., 2003a; Ignatov et al., 2003b). To find a receptor for HA, we concentrated on GPCR subfamilies reacting with small peptides as ligands.

Several orphan receptors failed to show interactions with HA, including GPR6 and GPR12, for which we found lysophospholipids as cognate ligands (Ignatov et al., 2003a;

degraded (Imai et al., 2001). To prevent aggregation and subsequent degradation, we integrated GPR37 stably into HEK-T-REx cells with a construct that allowed induction by tetracycline (HEK-T-REx–GPR37). Incubation of cells with the tetracycline derivative doxycycline for 24 hours resulted in production predominantly of the monomeric form of GPR37 (Fig. 2C, first lane). Without doxycycline induction, GPR37 was not detectable (Fig. 2C, second lane). Confocal image analysis revealed that, after induction with doxycycline, GPR37 localised mainly to the outer cell membrane, both in permeabilised (Fig. 2D) and non-permeabilised cells (Fig. 2F). The non-induced cells showed no GPR37 immunoreactivity (Fig. 2E,G). To study internalisation, HEK-T-REx–GPR37 cells were incubated in defined medium for 24 hours with doxycycline to induce GPR37 expression. Subsequent treatment with HA for 10 minutes led to rapid internalisation of GPR37 (Fig. 2H,I). This internalisation was much faster in HEK than in COS-7 cells, probably as a result of differences in -arrestin levels (Ménard et al., 1997).

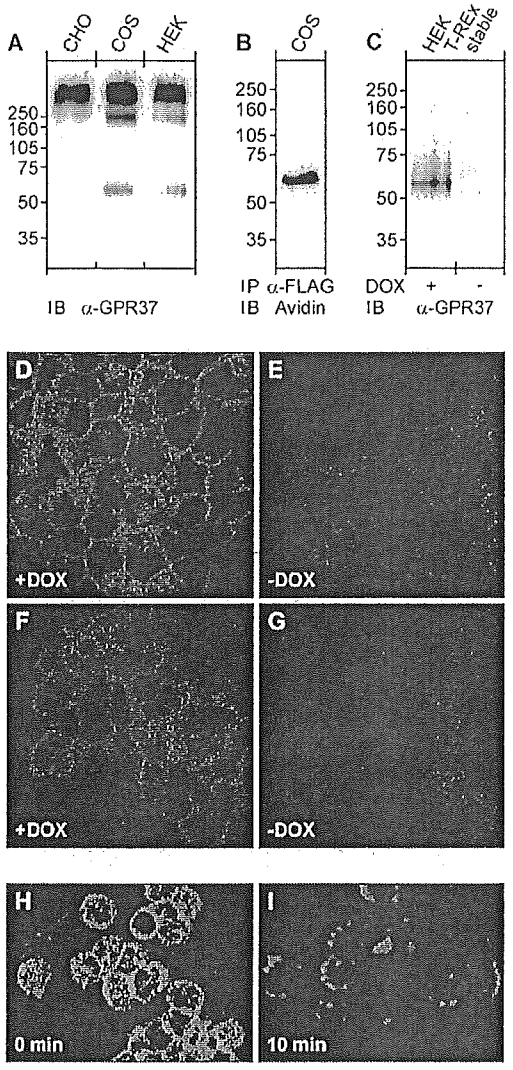

Fig. 2. Inducible, stable expression of GPR37 prevents aggregate formation. (A) CHO-K1, COS-7 and HEK-293 cells were transiently transfected with GPR37, and membrane fractions were assayed by immunoblotting (IB) with anti-GPR37 antibody (-GPR37). (B) COS-7 cells transiently transfected with GPR37-FLAG were cell-surface biotinylated, and the solubilised membrane fraction was immunoprecipated (IP) with anti-FLAG antibody (-FLAG) and visualised after immunoblotting with avidin. (C) GPR37 was introduced stably into the flip-in cell line HEK-T-REx, where GPR37 expression is inducible by doxycycline (DOX). Membrane fractions were subjected to western blotting with anti-GPR37 antibody (-GPR37) with (first lane) and without (second lane) induction for 24 hours with doxycycline. (D-I) HEK-T-REx–GPR37 cells with (D,F,H,I) and without (E,G) doxycycline induction for 24 hours were immunostained with anti-GPR37(R2) antibody after permeabilisation (D,E) and with anti-GPR37 antibody without permeabilisation (F-I). (H,I) HEK-T-REx–GPR37 cells were treated with 2 nM HA for 0 and 10 minutes at 37°C, respectively, fixed with 2% formaldehyde for 10 minutes and subsequently immunostained with anti-GPR37 antibody.

HA binds to GPR37

To show direct interaction of HA with GPR37, COS-7 cells were analysed after incubation with 2 nM HA by fluorescence resonance energy transfer (FRET). Localisation of HA was detected with a HA-specific polyclonal antiserum and was visualised with a Cy2-coupled secondary antibody (green). To detect GPR37, monoclonal antibodies directed against the extracellular domain of human GPR37 were used in combination with a Cy3-coupled secondary antibody (red). Fig. 3A-D shows a typical example of FRET between HA and ectodomains of GPR37. After bleaching a discrete area in a GPR37-positive cell (Fig. 3A,B), an increase in HA fluorescence was observed (Fig. 3C,D). The difference in staining pattern is due to the fact that COS-7 cells, in addition to GPR37, express endogenous HA receptor(s) (Boels et al., 2001). The experiment was repeated several times on different days yielding similar results. On average, the calculated energy-transfer efficiencies were in the range of 19.4±4.5%, indicating the close association of GPR37 and HA. Non-transfected cells were negative, and no transfer of signal was obtained if an antibody against the FLAG tag at the C-terminus of GPR37 was used (data not shown).

For visualisation of HA binding to GPR37, a fluorescent derivative of HA was produced. For this purpose, the fluorophore Cy3B was coupled to the -amino group of Lys7 of HA. The neuroblastoma cell line NH15-CA2, which reacts with HA (Ulrich et al., 1996) and endogenously expresses GPR37 (Fig. 3E), was used as positive control. Binding of Cy3B-labelled HA to NH15-CA2 cells was observed starting from a concentration of 50 nM, with optimal binding at 150 nM, achieved after incubation for 10 minutes at 37°C (Fig. 3F). Pre-incubation with unlabelled HA for 50 minutes prevented Cy3B-HA binding (Fig. 3G). Cy3B-labelled HA did not bind to HEK-T-REx–GPR37 cells without induction of GPR37 expression by doxycycline (Fig. 3H), but reacted after induction for 24 hours with doxycycline (Fig. 3I). Pre-incubation with unlabelled HA inhibited binding (Fig. 3J), demonstrating that the two ligands compete for the same receptor and that the receptor is either occupied or, more likely, internalised after interaction with HA.

HA induces an increase in Ca^{2+} mobilisation in cells expressing GPR37

To confirm the interaction of HA with GPR37, Ca^{2+} mobilisation was measured in CHO-K1 cells stably

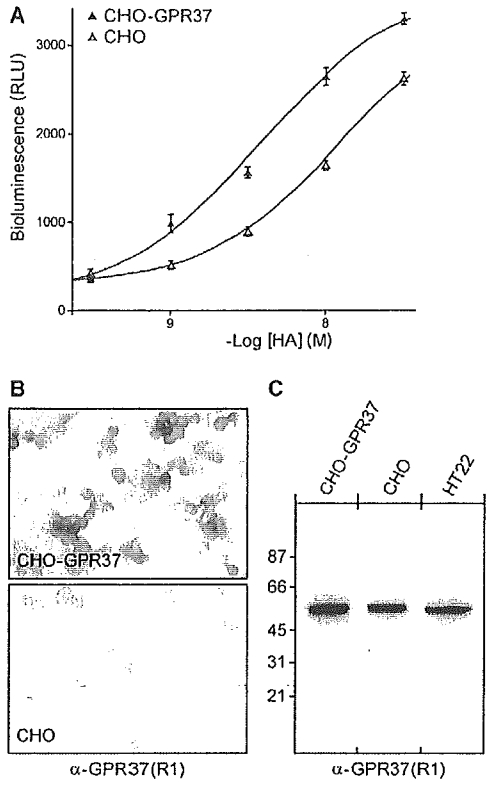

Fig. 4. HA stimulates Ca^{2+} mobilisation in CHO-K1 cells stably transfected with GPR37-FLAG, G 16 and apoaequorin. (A) The Ca^{2+}-bioluminescence response was measured at 469 nm and is expressed in relative light units (RLU), from which the medium response was subtracted. Values are given as means ± s.d. CHO-G 16-AEQ cells stably expressing GPR37-FLAG (CHO-GPR37) responded with an EC_{50} value of 3.3 nM; the endogenous response of CHO-G 16-AEQ cells (CHO) resulted in an EC_{50} value of 11 nM. Data show representative results of three independent experiments. (B) CHO-GPR37 (upper panel) and CHO cells (lower panel) reacted with anti-GPR37(R1) antibody [-GPR37(R1)], a polyclonal antiserum produced against the conserved intracellular C-tail. (C) Western blot analysis of membrane fractions confirmed an increased expression of GPR37 in transfected cells. The mouse hippocampal cell line HT22, expressing GPR37 endogenously, was used as a positive control.

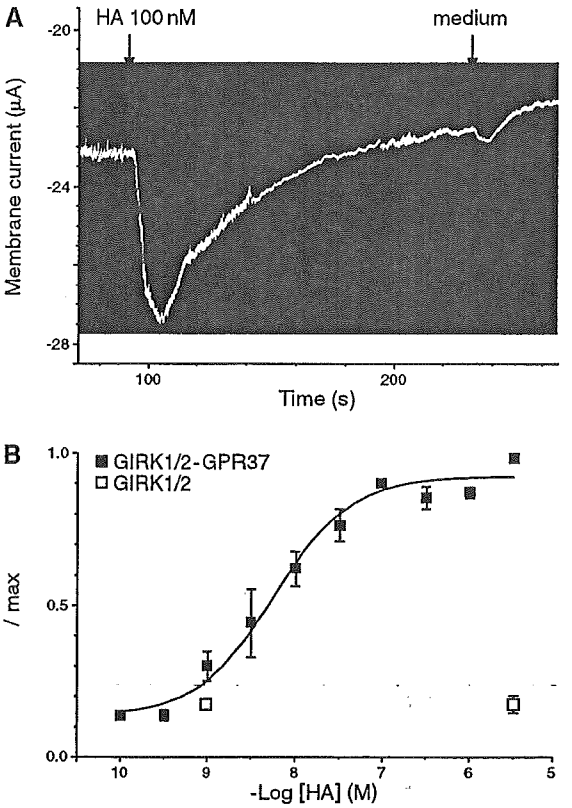

Fig. 5. HA is a high-affinity ligand for GPR37 expressed in frog oocytes. (A) Currents induced by 100 nM HA were recorded from *Xenopus* oocytes injected with cRNAs coding for GPR37 and for GIRK1/2. Stimulation with medium served as control. (B) The current increase was dependent on HA concentration. Dose-response curves for a HA-induced increase in GIRK1/2-mediated inward currents were normalised against maximal currents obtained for each oocyte. Current increases were averaged over four oocytes prepared and injected on the same day. The values represent means ± s.d. Data are representative of several independent experiments.

to an increase in membrane currents (Fig. 6B), which was blocked by La^{3+} and by SKF (Fig. 6B), both of which are known inhibitors of TRP-like Ca^{2+} channels. These Ca^{2+} channels, upon stimulation of receptors with ligands, translocate from an intracellular pool to the plasma membrane, for which activation of phosphoinositide 3-kinase (PI 3-kinase) and Ca^{2+}-dependent calmodulin (CaM) kinase is a prerequisite (Boels et al., 2001). The HA-induced increase in current was prevented by pre-incubating cells with pertussis toxin, wortmannin and KN93 (Fig. 6C), which demonstrates that an inhibitory G protein, PI 3-kinase and CaM-kinase II, respectively, are involved in the HA-GPR37 signalling cascade. A preliminary scheme of HA signalling is shown in Fig. 7.

Discussion

We present evidence that HA is a high-affinity ligand for GPR37. After heterologous expression in frog oocytes and in mammalian cells, EC_{50} values in the low nanomolar range were obtained. Electrophysiological analysis revealed that GPR37 activation by HA involved the same signalling cascade (Fig. 7) as found earlier for the endogenous HA receptor (Boels et al., 2001; Kayser et al., 1998; Ulrich et al., 1996). Interaction with HA resulted in GPR37 internalisation and stimulated entry into mitosis.

HA is bound to a carrier-like molecule both in hydra and in mammals, which improves the half-life and function of HA (Roberge et al., 1984; Schaller et al., 1996). The HA-binding protein HAB was isolated from hydra using HA-affinity chromatography, and later SorLA was discovered as an orthologue of HAB (Hampe et al., 2000). SorLA is a multi-ligand sorting receptor that, in addition to HA, binds glial-cell-derived neurotrophic factor (GDNF), PDGF and apolipoprotein E (ApoE) (Gliemann et al., 2004; Taira et al., 2001; Westergaard et al., 2004). HAB and SorLA are type I

Materials and Methods

Monomerisation of HA and synthesis of Cy3B-labelled HA

HA was from Bachem AG. Monomerisation was achieved by heating a 10 M solution of HA in 0.1 N HCl for 5 minutes to 95°C. After neutralisation with NaOH to pH 7.0, samples were stored frozen at –20°C and used 2-3 times only (Bodenmuller et al., 1986). For labelling Cy3B, 150 nmoles of monomerised HA were lyophilised and dissolved in 100 l dimethylformamide containing 0.2% *N*-methylmorpholine. Cy3B-mono-*N*-hydroxysuccinimide (NHS) ester (Amersham Biosciences) was dissolved in the same buffer (0.5 mg in 50 l) and incubated with HA overnight in the dark. The Cy3B-labelled HA was purified by C18 reverse-phase HPLC, yielding approximately 30-40 nmoles of Cy3B-labelled HA.

Molecular biology

Human GPR37 cDNA was inserted into pcDNA 3.1 (+) and into pcDNA3-FLAG-His6C as described earlier (Imai et al., 2001). GPR37 and GPR37-FLAG were subcloned into the dual-function vector pXOON, a kind gift from T. Jespersen, optimised for expression both in frog oocytes and in mammalian cells (Jespersen et al., 2002). GPR37-FLAG was introduced into CHO-K1 cells stably expressing G 16 and apoaequorin (CHO-G 16-AEQ) (Stables et al., 1997) with the vector pIRES-P, a kind gift from S. Hobbs (Hobbs et al., 1998). Stable integration was monitored by immunostaining with antibodies against FLAG (Sigma-Aldrich). For inducible expression, GPR37 was transfected into HEK-293 cells using the Flp-In T-REx system of Invitrogen (Karlsruhe, Germany). The concatemeric construct between GIRK1 and GIRK2 (GIRK1/2) was kindly provided by A. Karschin (Wischmeyer et al., 1997). All constructs were confirmed by sequencing.

Expression of GPR37 in *Xenopus laevis* oocytes and electrophysiology

For functional expression in frog oocytes, the GPR37 cRNA was transcribed in vitro with T7 polymerase from the *Xba*I-linearised pXOON-GPR37-FLAG vector and co-injected at a ratio of 5:1 with cRNA of the concatemeric GIRK1/2 construct transcribed from the *Nhe*I-linearised plasmid. For recordings, oocytes were superfused with ND-96 medium (96 mM NaCl, 2 mM KCl, 1.8 mM $CaCl_2$, 1 mM $MgCl_2$, 5 mM Hepes, pH 7.5). Two-electrode voltage-clamp recordings were performed with electrodes pulled to a tip resistance of 0.5-2.0 M . A Gene Clamp 500B amplifier (Axon Instruments), pClamp9 (Axon Instruments) and Origin (Microcal Software) served for data acquisition and analysis. Whole cells were clamped at –100 mV. For agonist measurements, the medium was changed to high K^+ (ND-96 with 96 mM KCl, 2 mM NaCl). After the initial inward current had reached a plateau, agonists were applied in high K^+ medium. Agonist treatment was terminated by wash-out with low K^+ to control intactness of the oocyte membrane. All recordings were performed at room temperature.

Cell culture, transfection and immunostaining

NH15-CA2, HT22 and COS-7 cells were cultured in DMEM supplemented with 10% fetal calf serum (FCS), HEK-T-REx-GPR37 cells with 10% newborn calf serum (tetracycline-free) and CHO-K1 cells in DMEM-F12 with 5% FCS. For routine culture, 100 U ml^{-1} penicillin, 100 g ml^{-1} streptomycin and 10 mM Hepes, pH 7, were added to these media. CHO-G 16-AEQ cells stably expressing GPR37 required the addition of 750 g ml^{-1} geneticin, 200 g ml^{-1} hygromycin and 5 g ml^{-1} puromycin. HEK-T-REx-GPR37 cells were induced to express GPR37 by incubation in 1 g ml^{-1} doxycycline. Lipofectamine 2000 (Invitrogen), Fugene 6 (Roche Diagnostics), or electroporation were used for transfection. To assay ligands, cells were transferred overnight into serum-free defined medium consisting of the respective basal media to which 5 g ml^{-1} insulin, 30 g ml^{-1} transferrin, 20 M ethanolamine, 30 nM sodium selenite, 1 M sodium pyruvate, 1% non-essential amino acids and 2 mM glutamine were added.

For immunocytochemistry, cells were fixed either with 4% formaldehyde in PBS for 30 minutes at room temperature or with ice-cold 1% acetic acid in ethanol for 5 minutes. After washing with 0.1% Triton X-100 and pre-absorption with 1% bovine serum albumin, first and second antibodies were applied. For cell-surface staining, living cells were incubated with ligand and/or antisera for 20-30 minutes on ice, washed, fixed and visualised as indicated. No Triton X-100 was added to prevent permeabilisation. For western blotting, cells were harvested by treatment with 2 mM EDTA in PBS for 10 minutes, collected by centrifugation, and ultrasonicated for 20 seconds in Tris-HCl buffer, pH 7.4, containing 2 mM EDTA and a protease-inhibitor cocktail (Roche Diagnostics). After centrifugation at 100,000 *g*, the membrane pellets were dissolved in sample buffer and separated by SDS-PAGE. The monoclonal mouse anti-GPR37 antibody, recognising an extracellular domain of recombinant human GPR37, was used at a dilution of 1:400, the polyclonal rabbit antisera against the intracellular C-terminal domain of GPR37, anti-GPR37(R1) and anti-GPR37(R2), were diluted 1:1000 and 1:2000, respectively. All GPR37-specific antibodies were produced in the laboratory of Takahashi and have been described previously (Imai et al., 2001). The antibody against FLAG (M2) was from Sigma-Aldrich and that against phospho-histone H3 from Biomol. Cy2 or Cy3 secondary antibodies were used for confocal analysis, and alkaline phosphatase- or peroxidase-conjugated secondary antibodies were used for light microscopy and western blotting. Western blots were visualised by ECL. Biotinylated proteins were detected with an avidin-peroxidase conjugate (Bio-Rad).

FRET analysis

For fluorescence resonance energy transfer (FRET) experiments, HA was reacted with the highly specific HA antiserum 102.8, which binds to HA in the picomolar range and was described earlier (Schaller et al., 1984). It was used at a dilution of 1:3000 and visualised with Alexa Fluor 488 goat anti-rabbit as donor (Invitrogen). GPR37 was detected with anti-GPR37 antibody and visualised with Cy3 anti-mouse antibody (Amersham) as acceptor. The energy transfer was detected as increase in donor fluorescence (Alexa Fluor 488) after complete photobleaching of the acceptor molecule (Cy3). Initial images were recorded after excitation at 488 and 568 nm. A discrete area of the sample was illuminated with intense 568 nm light (laser power 100%) for a few minutes to destroy completely the acceptor fluorescence. The cell was then rescanned using excitation at 488 nm. An increase within the photobleached area was used as a measure for the amount of FRET obtained. The efficiency of energy transfer (E) was expressed as E=1-(D1/D2), where D1 is the donor fluorescence before, and D2 after, photobleaching. Data were collected for 4-5 different fields from a single coverslip; 2-3 coverslips were used for each measurement; the experiment was repeated at least three times.

Biotinylation of surface proteins

COS-7 cells were transiently transfected with GPR37-FLAG using the Fugene 6 reagent (Roche Diagnostics). 48 hours after transfection, cells were washed 2 with PBS and biotinylated for 30 minutes at room temperature with 1 mM S-NHS-biotin (Perbio Science). The reaction was stopped by addition of 0.5 M Tris-HCl, pH 7.5, for 5 minutes at room temperature, and the cells were washed with PBS to remove free biotin. Cell lysates were prepared in a buffer consisting of 5 mM EDTA, 10 mM Tris-HCl, pH 7.4, and protease-inhibitor cocktail. Samples were ultrasonicated for 20 seconds and centrifuged at 100,000 *g* for 30 minutes. Pellets were solubilised in buffer containing 1% Triton X-100, 0.5% NP40, 150 mM NaCl, 7 mM EDTA, 1 mM EGTA, 10 mM Tris-HCl, pH 7.4, and protease-inhibitor cocktail for 30 minutes on ice, followed by centrifugation at 16,000 *g* for 15 minutes at 4°C. The supernatant was used for immunoprecipitation.

Immunoprecipitation with anti-FLAG M2-agarose

Since high concentrations of NP40 inhibited binding to FLAG-agarose, the supernatant from the NP40-solubilised and biotinylated COS-7 cells was diluted fivefold with TBS (150 mM NaCl, 50 mM Tris-HCl, pH 7.4) to reduce the NP40 concentration to 0.1%. Samples were incubated with 100 l anti-FLAG M2-agarose (Sigma-Aldrich) overnight at 4°C and then centrifuged at 1500 *g* for 5 minutes at 4°C. Pellets were resuspended in 1 ml TBS and centrifuged again at 16,000 *g* for 2 minutes at 4°C. After washing with TBS, pellets were dissolved in 50 l sample buffer and subjected to western blotting.

Electrophysiology with mammalian cells

For electrical recordings, COS-7 cells were microinjected with 50 ng l^{-1} GPR37-pcDNA3 and 5 ng l^{-1} EGFP-N1-pcDNA3, the latter being used to facilitate detection of successfully transfected cells. Membrane currents were recorded in the whole-cell configuration of the patch-clamp technique (Hamill et al., 1981) or the perforated-patch configuration with nystatin (Horn and Marty, 1988). An EPC9 patch-clamp amplifier was used in conjunction with the PULSE-stimulation and data-acquisition software (HEKA Elektronik). The patch electrodes were made from 1.5 mm diameter borosilicate glass capillaries with resistances of 2.5-4 M . Data were low-pass filtered at 3 kHz and compensated for both fast and slow capacity transients. Series resistance was compensated by 75-90%. All experiments were performed at room temperature (22-25°C). The pipette solution contained 140 mM KCl, 2 mM $MgCl_2$, 1 mM $CaCl_2$, 2.5 mM EGTA, 10 mM HEPES and had a calculated free Ca^{2+} concentration of 66 nM. The pH was adjusted to 7.3 with KOH. The standard external solutions contained 140 mM NaCl, 2 mM $MgCl_2$, 2 mM $CaCl_2$, 5 mM KCl, 10 mM HEPES and 10 mM glucose, buffered to pH 7.3 with NaOH. Nystatin was dissolved in dimethyl sulfoxide (DMSO). Its final concentration in the standard pipette solution was 0.2 mg ml^{-1}. All chemicals for electrophysiology were purchased from Sigma-Aldrich.

Statistical analysis

The results are expressed as means of 3-6 determinations ± s.d. Curve fittings were performed with the Prism program (GraphPad). Each experiment was repeated at least three times.

We thank T. Jespersen for providing the vector pXOON, S. Hobbs for pIRES-P, A. Karschin for the concatemeric GIRK1/2 construct, J. Stables for the CHO-G 16-AEQ cell line and S. Hempel for help with the figures.

Regular Article (NBD-05-378-Revised)

Conditional knockout of Mn superoxide dismutase in postnatal motor neurons reveals resistance to mitochondrial generated superoxide radicals

Hidemi Misawa,[a,b,*] Kazuko Nakata,[a] Junko Matsuura,[a] Yasuhiro Moriwaki,[b] Koichiro Kawashima,[b] Takahiko Shimizu,[c] Takuji Shirasawa,[c] and Ryosuke Takahashi[d,e]

[a]Department of Neurology, Tokyo Metropolitan Institute for Neuroscience, 2-6, Musashidai, Fuchu-shi, Tokyo 183-8526, Japan

[b]Department of Pharmacology, Kyoritsu University of Pharmacy, 1-5-30, Shibakoen, Minato-ku, Tokyo 105-8512, Japan

[c]Department of Molecular Gerontology, Tokyo Metropolitan Institute of Gerontology, 35-2, Sakae-cho, Itabashi-ku, Tokyo 173-0015, Japan

[d]Laboratory for Motor System Neurodegeneration, RIKEN Brain Science Institute, 2-1, Hirosawa, Wako-shi, Saitama 351-0198, Japan

[e]Deparment of Neurology, Graduate School of Medicine, Kyoto University, 54, Sho-goin kawaramachi, Sakyo-ku, Kyoto 606-8507, Japan

*Corresponding author. Department of Pharmacology, Kyoritsu University of Pharmacy, 1-5-30, Shibakoen, Minato-ku, Tokyo 105-8512, Japan

Tel. +81-3-5400-2675

Abstract

Mitochondrial dysfunction and oxidative damage are implicated in the pathogenesis of neurodegenerative disease. Mice deficient in the mitochondrial form of superoxide dismutase (SOD2) die during embryonic or early postnatal development, precluding analysis of a pathological role for superoxide in adult tissue. Here we generated postnatal motor neuron-specific SOD2 knockouts by crossing mice with floxed SOD2 alleles to VAChT-Cre transgenic mice in which Cre expression is restricted to postnatal somatomotor neurons. SOD2 immunoreactivity was specifically lost in a subset of somatomotor neurons resulting in enhanced superoxide production. Yet extensive histological examination revealed no signs of oxidative damage in animals up to 1 year after birth. However, disorganization of distal nerve axons following injury was accelerated in SOD2-deficient motor neurons. These data demonstrate that postnatal motor neurons are surprisingly resistant to oxidative damage from mitochondrial-derived superoxide radicals, but that such damage may sensitize axons to disorganization following nerve injury.

Key Words: Motor neurons; Oxidative stress; Mitochondria; Nerve injury; Conditional knockout; SOD2; Amyotrophic lateral sclerosis

background. SOD2 knockout mice on a CD-1 background die either in utero or within 24 hours after birth from severe dilated cardiomyopathy (Li et al., 1995). Similarly, C57BL/6 SOD2 knockout mice die at late embryonic or early neonatal stages from dilated cardiomyopathy (Huang et al., 2001; Ikegami et al., 2002). On a mixed C57BL/6 and 129/Sv background, SOD2 mutant mice survive for up to 18 days, develop a milder-form of dilated cardiomyopathy and display a neurological phenotype (Lebovitz et al., 1996). In contrast, DBA/2J (D2) SOD2 mutant mice do not develop cardiomyopathy but instead develop severe metabolic acidosis and survive an average of 8 days (Huang et al., 2001). This phenotypic variation suggests that sensitivities to SOD2 deficiency are highly dependent on genetic modifiers that differ across strain and cell type.

Motor neurons are believed to be particularly susceptible to oxidative damage given the high metabolic requirement to sustain a large cell size and long axonal processes. Although motor neurons in cell culture are vulnerable to cell death mediated via calcium influx after exposure to glutamate, it is unclear how motor neurons respond to the overproduction of mitochondrial-derived ROS in vivo. To circumvent the early lethality of SOD2 knockout mice, we used a conditional gene deletion approach in which mice with floxed SOD2 genes (Ikegami et al., 2002) were mated with VAChT-Cre mice (Misawa et al., 2003) that express Cre recombinase in approximately 50 % of postnatal somatic motor neurons. Here we report that conditional loss of SOD2 in postnatal motor neurons results in elevated mitochondrial oxidative stress that fails to triggers signs of neurodegeneration under non-pathological conditions. In contrast, nerve axotomy revealed accelerated nerve disorganization, suggesting that adult motor neurons have relative resistance to mitochondrial-generated